TEMPLATE
BUKU PROFIL PENYELIDIKAN SKIM GERAN PENYELIDIKAN FUNDAMENTAL (FRGS) FASA 1/2015 DAN FASA 2/2015

INVESTIGATION OF MICRO-EXPLOSION PHENOMENON IN THE COMBUSTION OF TRI-FUEL (DIESEL, BIODIESEL AND BIO-ETHANOL) EMULSION IN COMPRESSION IGNITION ENGINES

Ftwi Yohaness Hagos
Rizalman Bin Mamat
Abdul Adam Bin Abdullah
Amir Bin Aziz
Ahmed Nurye Omer
Abd. Rashid bin Abd. Aziz
Automotive Engineering Centre
ftwi@ump.edu.my
FRGS Field

ABSTRACT (120 words)

The current research is aimed at investigation the micro-explosion phenomenon of a tri-fuel emulsion in compression ignition (CI) engine. Alcohols and biodiesel to be emulsified in diesel fuel at different proportions for an improvement in the combustion, performance and emission through the manipulation of the micro-explosion phenomenon. In its initial stage, the research planning was limited to preparation stage where the main activities in this stage are literature review and preparation of equipment and materials. Optimization of the ultrasonic emulsifier for the emulsion preparation by varying the amplitude, the pulse and time of emulsion has been conducted to see the effect of the stability of the emulsion. Besides, the stability and fuel characterization of different proportion of component fuels has been investigated and an article is in the review process.

Comparison between the emulsion and blending was studied. A setup for the spray characterization and compression ignition engine is ready. Onset of micro-explosion phenomenon is investigated. The spray penetration comparison of different emulsified fuels and diesel fuel are compared. Besides, the spray spread, the droplet size, spray cone and spray dispersion and their relationship with the physico-chemical characteristics of the emulsified fuel is done. Flame visualization: Flame visualization has become a challenge on the progress of the study. The chamber is equipped with visualization window. the glass being used for the visualization is BK glass where it can only withstand temperature of 700 K. Therefore, the glass breaks when combustion is initiated. Therefore, the experiment is limited to spray characterization and investigation of micro-explosion phenomenon. The combustion and emission study is completed. The effect of emulsification on the combustion, performance and emissions was investigated and their relationship with the physico-chemical characteristics of the emulsified fuel is done. The OPEN FOAM modeling, nozzle geometry is prepared, meshing is completed and setting up boundary and governing equations ongoing. The modeling work is completed. Model validation was done with the help of the experimental data. There is a strong agreement.

1. INTRODUCTION

Fossil fuel demand is increasing (BP, 2017; Martins, Felgueiras, Smitkova, & Caetano, 2019; Tran, 2019). It is expected that between 2020 and 2030, the irreversible decline of global fossil fuel production per capita is forecasted (Nehring, 2009). According to the estimation in view of BP 2015 statistic review, there are less than 44 years of oil remaining with primary oil fields now already started demonstrating production decreasing (Leopold & Hutchins, 2016). Again, BP 2017 statistics has revealed a decreasing pattern on world oil production and with a slight increase in reserve. Nevertheless, the calculated figure has suggested that the reserve is sufficient for 50.6 years of current production (BP, 2017). According to ExxonMobil, through 2040, diesel demand is expected to account for at least 70% of all transportation fuel growth.

One of the prominent fossil fuel is diesel used in compression ignition engine. Perceptively controversial however the engine is versatile and has been in many applications because of the durability. However, the engine emission is the main limitation which challenging its existence. The concentration of gas emission in the city is identified to be the main concern. Especially in the urban area, the air quality problem is found to be concentrated. The diesel engine is still in high demand considering running with diesel fuel is much more efficient and cheaper than running with petrol.

The gases that contribute the most from the combustion of the CI engine includes unburned hydrocarbon (HC), Nitrogen oxide (NO_x), carbon monoxide (CO) and carbon dioxide (CO_2). CO is colourless gas with the same density as air and could replace oxygen from blood caused by incomplete combustion. In theory, CO_2 and water are converted from the combustion of diesel fuel. However, due to impurity and imperfection of combustion, CO is produced and react with oxygen and producing CO_2. An excessive amount of CO_2 in the long term may affect global climate change. CO_2 excessive emission comes from fossil fuel combustion (Höök & Tang, 2013). The increase in CO_2 and NO_x are a lethal combination. NO_x actually poisoners and have been linked by the health organization to a serious respiratory condition. Originally, mitigation from a petrol engine to the diesel engine is because of CO_2 reduction. This seems like a solution at first but actually not. To counter this, emission regulation implemented strict emission standard and continuously pressuring engine manufacturer to act upon the issue. By the year 2021, heavily regulated, the expectation of NO_x emission will be set to become 1/10th of today limit (Santini, Gosala, & Shaver, 2016).

Traffic congestion is one of the root cause of air pollution. Moreover, there is an increasing concern that the compression ignition (CI) engine is one of the significant ignition sources with immense air pollution contributor to one extent. Exposure to the diesel engine emission is a potential risk associated with a health problem such as the risk of brain damage, increased of cardiovascular illness, lung cancer and heart diseases (Costello et al., 2018; Nemmar et al., 2003; Neophytou, Picciotto, Costello, & Eisen, 2016; Poulsen, Sørensen, Andersen, Ketzel, & Raaschou-Nielsen, 2016; S. Yang & He, 2016). Although individual transport vehicles with diesel fuel-powered may seem like minor suspects at one glance. Nevertheless, the statistic on pollution watch revealed otherwise. World demand for transport fuel alone accounts for 60% of world oil consumption with a market share of a vehicle with a diesel engine in some of the

European countries have exceeded 60% (Hegab, La, & Shayler, 2016). Particularly, heavy engine class and passenger vehicle run on diesel correspondingly accountable due to the expected demand increase by 85% between 2010 and 2040 (Hegab et al., 2016). Consequently, a heavy-duty diesel engine shared the highest portion of NO_x to the scenario (Y. Kim, Han, & Sohn, 2017). Agricultural and construction sector widely attached to the heavy-duty application of diesel power machinery. Subsequently, the demand for diesel is higher as compared to gasoline due to the wider scope of diesel engine application, unlike gasoline engine which is only for transportation (Abu-Hamdeh & Alnefaie, 2015).

A recent study proposed a new model of demand forecasting. The model suggests an engine manufacturer to consider reducing the production of the heavy-duty diesel engine in responding to the rise of the next-generation technology. The technology that could cope with the upcoming wave of strict emission regulation (Y. Kim et al., 2017). To expect new technology such as an electric car or hybrid engine to immediately replace CI engine is not yet feasible. In addition, prompt oil price drop as a result of such technology rise can still be considered unrealistic. Some of the current hybridization disadvantages include the no improvement in rate battery capacity, the additional cost of a battery, weight increase, the intricacy of the vehicle system and the complex control system (Pollet, Staffell, & Shang, 2012). Dispelling myths, high electricity consumption will only indirect causing more fossil fuels to be burned. In the end, it all brings back to square one. Furthermore, mass production and the use of hybrid or electric car are seemingly not the solutions yet considering electric vehicle battery with doubt rely on the availability of the “critical metal” known as lithium (Speirs, Contestabile, Houari, & Gross, 2014).

Fossil fuel has been identified harming the environment and may be possible to run out in the future. Hence, the world is now inclined to shift into renewable sources such as biofuels. While global climate protection is the responsibility of all, it is the risk that requires sharing act and creative solutions.

The source of biofuel is widely available and potentially has a lot to offer. Unfortunately, it has not been fully utilized specifically as a source of energy for the engine. Malaysia for example with large feedstock source such as palm oil promote value to remove biofuel technology barrier associated with the energy source for the engine. Lately, the Malaysian Palm Oil Board (MPOB) is seen in full swing to improve the palm oil industry. On the light of that, mix approach with biodiesel, bioethanol and diesel received interest. The mixed fuel approaches up to three compositions or known as tri-fuel will not only be addressing the air pollution and lessen down total dependency on fossil fuel but also potentially capable of boosting the trade and development between nation. A number of mitigation strategies that have already been the topic of research interest such as water in diesel, fuel additive as well as bi-fuel indirectly inspired the idea of tri-fuel and has begun to appear in the literature.

Currently, bioethanol has no market in diesel engine fuel for the transportation sector. The second generation of ethanol use biomass which can boost rural economy unlike the primary generation of ethanol from starch content such as cone, sugar cane or many more which competes with the food source. The discouragement is understandable since while the number of people dying on food hunger in someplace increases, to utilize the source for fuel production does not make sense, not recommended and a non-ethical.

Moreover, since the limit factor is viscosity and oxygen content, NO_x emission will be expected to be higher with beyond 20% biodiesel input. With less than 20% biodiesel, the performance is almost on par with conventional diesel but to go beyond, the performance may decline. The same is true with ethanol-diesel blend optimization benchmark up to 15%. Together in the tri-fuel application, the replacement can be possible to achieve up to 30% (S. A. Shahir et al., 2014). Especially in Malaysia context on job creation and with national energy security, tri-fuel is worth counting on and will be one of the strategic action. In addition, Malaysia was previously fuel exporter country and now the inclination is shifting slowly towards fuel import country. Holistically, what tri-fuel could contribute locally would be a dependency on import may reduce and perhaps export more. Furthermore, commercialization of locally available resource could contribute to more job creation especially covering rural areas.

CI engine combust differently compared to the SI engine. The process is unsteady and the technical limitation of the diesel engine is on the spontaneous flame coming from heterogeneous charge mainly with respect to excessive formation of particulate matter, smoke and NO_x formation. Narrow down further, exploring the possible attribute of tri-fuel emphasis on the backbone of compression ignition engine principle is substantial. Apart from responding to the issue of crude oil reserve limit, dependency and oil price fluctuation, fuel quality control improvement is also the aim of the environmental and human health as the ground foundation. The challenge is not just to make tri-fuel applicable in the existing CI engine with little or no engine modification but also to make it more efficient than singular conventional diesel fuel. One way is by re-examining the vital transformation phase of a tri-fuel droplet from liquid to gas form which can be considered essential in compression ignition principle. In the current CI engine operation, especially at high speed, even with diesel fuel, insufficient time for all liquid droplet to burn completely has been recognized as default drawback of combustion. Some of the fuel is unburned and undesirably reduced to particle carbon soot which needs to be addressed creatively. This unresolved blessing in disguise limitation might possibly be the crucial advantage with tri-fuel as an alternative fuel for CI engine. Tri-fuel tributary on the atomization process which happens before the combustion moment in the chamber starts could be the novelty solution. That intricate moment in the combustion chamber is known as secondary atomization involving puffing and micro-explosion phenomenon.

Further research in this area is needed to uncover the occurrence of micro-explosion phenomenon with tri-fuel emulsion in CI engine and to better understand the impact of the event on engine outcome.

2. RESEARCH METHODOLOGY

2.1. Physicochemical Properties Characterization

2.1.1. Density test

The density of all samples was measured at 20 ± 1°C using a portable density/specific gravity meter model DA-130N with supplied sampling nozzle vertical to the ground. The measuring method of the tool is resonant frequency oscillation, which was specified in ASTM D777, the standard test method of density by portable density meter. The measuring range capability of the density meter is from 0.0000 to 2.0000 g/cm3 with a resolution 0.0001 g/cm3 and accuracy ±0.001 g/cm3. After the emulsification procedure took place, the samples were allowed to cool down to 20°C in a mini refrigerator before measurement procedure took place. To avoid ethanol content in tri-fuel emulsion from evaporation, the prepared samples was contained in a tightly close plastic screw cap glass laboratory bottle. The procedure was repeated three times with average value obtained as the final reading to minimize the effect of systematic errors.

2.1.2. Viscosity test

Viscosity is a measure of resistance of fluid to the deformation produced by a shear stress. Brookfield, DV-III Ultra Programmable Rheometer was used for the viscosity test. Software used was Brookfield Rheocalc V3.3 Build 49-1. Properties tested was in accordance to the petroleum standard ASTM D445 (Suhaimi et al., 2018). Dynamic viscosity was measured according to the Equation 2.1; -

$$\mu = \tau \times \frac{dy}{dc} \qquad 2.1$$

μ = dynamic viscosity of fluid (N s/m^2)

τ = shear stress in fluid

dc = unit velocity (m/s)

dy = unit distance between layers (m)

dc / dy = shear rate (s^{-1})

Viscosity reading were taken under laminar condition (only directed by the shearing force) and average reading were taken within the detected equivalent range of 10% to 100% torque reading for any combination of spindle speed rotation. Temperature of each sample was recorded at initial stage spindle rotation starts at 40°C ± 1°C. Experiment was executed immediately after each preparation of sample with at least three repetitions. Maximum acceptable value of diesel standard viscosity according to ASTM D7467 is 4.1 cSt (Ali et al., 2015). Table shows primary program setting used for the viscosity test. Results from the original unit was converted to the unit of centipoise (cP) for analysis.

Table 1 Primary insert program setting for Rheometer

Primary setting	**CMD**	**Parameter set**	**Description**
Set Speed	SSN	10	Run the Rheometer at the specified speed
Loop start count	LSC	25	Mark the start of the loop
Wait for time	WTI	15	Remain at the steps until the specified time interval (mm:ss) has elapsed
Speed increment (+/-)	SSI	10	Increment or decrement the current speed by the specified value

2.1.3. Surface tension test

For surface tension test, Tension meter, Data Physics/ DCAT 9T software was used. Method of surface tension measurement that was chosen was Wilhelmy thin plate and ring method test was used for countercheck result validity. Wilhelmy equation was applied as expressed by the equation 2.2. The stage moved down the plate down towards the surface of the liquid until the meniscus connects with it. The Tensiometer measured the force acting on the plate due to its wetting. The force (F) needed to detach it from the surface of the liquid is expressed as eEquation *2.3* where cos θ was equal to 1 considering as

the plate was wet completely to achieve 0.1% accuracy. Surface tension acts on both sides of the plate, hence multiplying by two was needed. The same goes to the ring method, where the surface tension was multiplied by two because the it acts on the inside and outside circumference of the ring. The ring inner and outer radii were assumed equal considering the ring was precisely thin manufactured for the equipment. The total force needed to detach the ring (Total weight) is expressed in the equation *2.4*. Humidity and room temperature were controlled at 50% and 25 ± 1°C, respectively. Experiment was executed immediately after each preparation of sample with at least three repetitions. Properties tested was in accordance to the petroleum standard ASTM D971.

$$\gamma = \frac{Total\ Weight - Plate\ weight}{2 \times \cos\theta} \tag{2.2}$$

$$F = Total\ Weight = Plate\ Weight + 2\, l \cos\theta \tag{2.3}$$

$$F = Total\ Weight = Wradius + 4\pi R\gamma = 2\, l\, \gamma \tag{2.4}$$

Surface tension is the tensile force acting on a liquid surface of the fuel. At the surface, the bond is extra tight due to the stretching between molecules. Compared to the surface and the inner area, the bond strength is unbalance and yield stronger tension. The area at the surface is reducing due to the tendency of the attraction force known as surface tension.

2.1.4. Average droplet size test

Average droplet size can be obtained with Zetasizer machine [39][40]. Hence, the measurement to obtain the average droplet size of the 20 samples was done using Zetasizer Nano S90 machine. It is determined by measuring the Brownian motion of the droplet in the sample. By definition, Brownian motion is the random movement of particle in the liquid as a result of surrounding bombardment motion of other particle around (Sales & Support, 2014). Hence, by measuring the movement speed of the particle undergoing Brownian motion, the droplet size can be determined via dynamic light scattering (DLS) system (Fischer & Schmidt, 2016). Stokes-Einstein equation defined that relationship between the speed of the Brownian motion and the particle size at uniform temperature. Since DLS technique takes advantage of Brownian motion, the experiment cannot be conducted with unstable temperature or warm fresh made tri-fuel emulsion due to rapid motion of Brownian caused by the warm temperature. Nevertheless, within 24 hours prior to preparation, all the samples were measured with samples temperature at 25 ± 1°C. At such stable temperature, basic principle of DLS can be applied. In principle, slow Brownian motion means large particle while rapid Brownian motion means smaller the droplets.

High-density glass covet was used instead of disposable low-density plastic covet as the standard container. This was to avoid possible low density plastic covet material to encounter surface degradation due to chemical reaction with tri-fuel emulsion which consequently may affected the scattering light. Disposable micropipette was used to carefully pour sample into the high-density glass covet. Size measurement dedicated by the machine is 0.3 nm to 10 microns. The detector in Zetasizer ZS90 is installed at an angle of 90^0 to the path of incident light. Thus, it receives more scattered light compared to backscattering set-up where the angle is usually between 173^0 and 175^0.

2.1.5. Stability test

Stability test was conducted using a gravitational approach (Reham et al., 2015) and the method was adopted and modified from previous studies (Bahrudin et al., 2019; Corral-Gómez et al., 2019; Kwanchareon et al., 2007; K. H. Lee et al., 2017; Low et al., 2017; S. Fernando & M. Hanna, 2013). A volume of 500 ml per each sample was prepared and 16 ml for each was carefully poured into the test tube using the micropipette and properly sealed with aluminium foil for stability test. Two set of test tube for each sample were prepared to ensure the repetitive result. Tube test rack under close cap condition was used under room temperature between 24°C and 36°C. Humidity recorded was between 40% and 80%. The samples were left under gravitational force and daily observation was done for any separation. Observation was conducted for a total period of 100 days. Daily observation was executed for the first two weeks. Weekly observation after that and monthly observation after completed one-month cycle.

2.1.6. Morphology

Qualitative analysis on micro-structural configuration and feature of tri-fuel emulsion was executed with digital microscope. The method was adopted and modified from the previous study (Fernando & Hanna, 2004; Mehta et al., 2012; Tan et al., 2017). The experiment was relying on the interaction of samples with a visible light coming from below the sample stage as probe. A two-dimensional image was captured and process by open source image processing software available called ImageJ and Motic. The morphology study compliment the Average Droplet size distribution mentioned in the previous section.

Human eye is limited in many respects and hence, the use of digital microscope could assist in the analysis. The scale that correspond to the visibility of the sample for analysis can be macrostructure, mesostructured, microstructure and nanostructure. The study is restricted to cover the scale of microstructure. Characteristics feature detection concern was homogeneity or inhomogeneity prone, geometrical formation, droplet size, dispersed droplet within the capsulation, capsulation boundary region, interaction behaviour between droplets capsulated such as collision sequence, any dislocation substructure and droplet size distribution. Digital microscope brand Dolomite Calestron was employed with 5X,10X and 40X objective lens and the total magnification of the images was up to 400X. Samples were observed immediately after prepared within less than 1 hour. The micro-structural observation was further investigated after the tri-fuel emulsion has passed through the fuel injector. After injection, Microscope (BX51, Olympus, Model U_LHOOL-3, Tokyo, Japan) was used with 50X magnification and 10 μm depth of field. Software for droplet counting was done by using Motic software.

2.2. Experimental configuration for micro-explosion investigation

The experimental work was conducted in the Center for Automotive Research and Electric Mobility (CAREM) at Universiti Teknologi Petronas (UTP). The method was adopted and modified from the previous studies (O. Armas et al., 2011; Avulapati et al., 2016, 2019; Corral-Gómez et al., 2019; Y Liu et al., 2010; Yu Liu et al., 2015; Tanaka, Kadota, Segawa, Nakaya, & Yamasaki, 2006).

Limitation of the previous study was that the droplet is subjected to contact on a solid surface. The droplet distortion and disintegration were observed in the previous studies due to contact on the hot surface and secondary atomization were not purely generated. Hence, the setup for the second objective of the study as shown in Figure was adopted taking the limitations of the previous studies.

The setup is composed of five main components as follow: -

- Optical accessible constant volume chamber
- Droplet generator/ Fuel injection system,
- Temperature/ pressure monitoring and control system
- high speed camera with LED lighting.

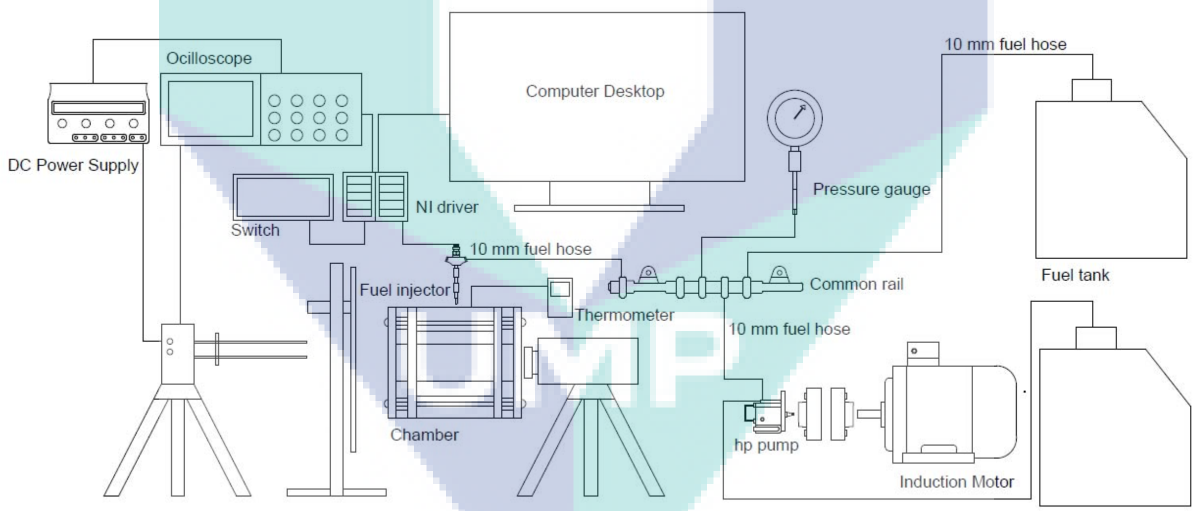

Figure 1 Schematics of Micro-explosion study setup

2.2.1. Optical accessible constant volume chamber

Optical accessible constant volume chamber was customized, designed and fabricated in a cylindrical shape with two channel optical accessible windows using computer numerical control (CNC) lathe and milling machines. Two of which were used for camera view and lighting source access. Two narrow holes were drilled on the side of the cylindrical chamber for the fuel injection and for the real-time temperature measuring thermocouple. Stainless steel was used as the core material considering the high melting point around 1510°C. The cylindrical shape chamber is assembled with easy to move viewport shutter both side for high temperature resistance glass installation. Figure shows disassemble optical accessible constant volume chamber consist of flange, heating element and mounting bolts. The optical heat resistance glass was made of fused silica material with high melting temperature, approximately at 1650°C and low thermal expansion. It was isolated from the metal flange through a heat resistant washer made of Teflon and fibreglass as shown in the Figure . The combination of Teflon and fibreglass as washer safeguards the optical glass from excessive force exerted by the fastening of the screws. Fibreglass was used considering the high resistance capability with melting point of 1121˚C. Flanges with each has five sets of mounting bolt serves as the optical glass attachment. Figure shows complete assembled constant volume chamber with installed fuel injector.

Figure 2 Disassemble optical accessible constant volume chamber

Figure 3 Fibreglass, teflon and optical glass for optical accessible constant volume chamber

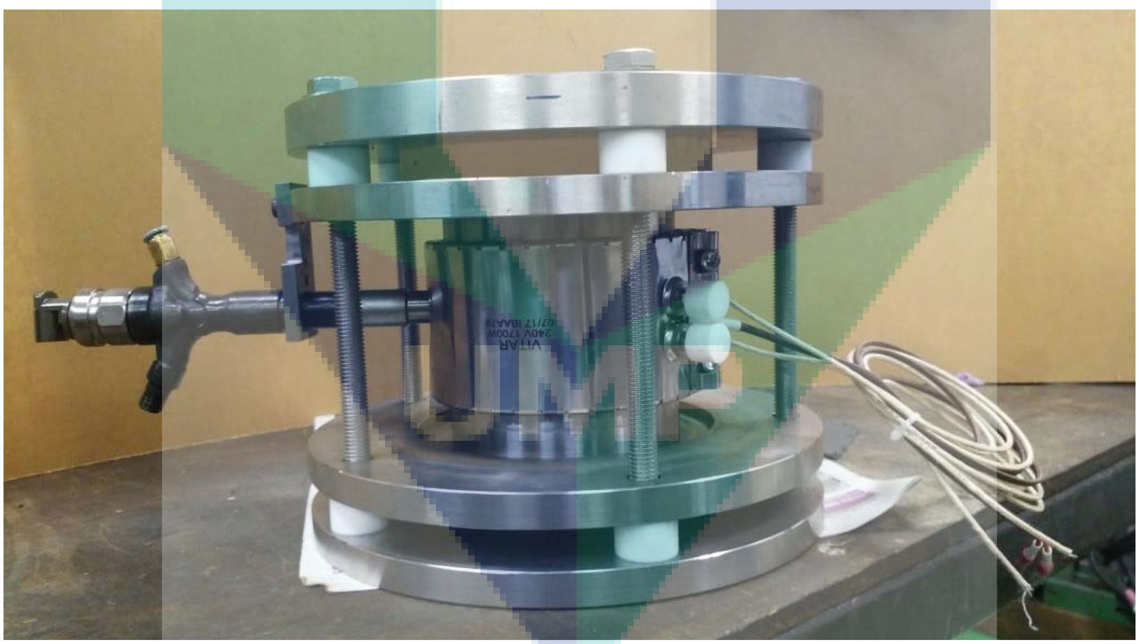

Figure 4 Assembled constant volume chamber with installed fuel injector.

A customized heater was manufactured by VITAR as shown in the Figure . It was made of ceramic specially band heater designed in light weight for uniform heat transfer to the chamber. The model is 07/17 IBAA78 is with capability of receiving 240 V and 1700 W. Figure shows the power supply for the heating source.

Figure 5 Customized heater

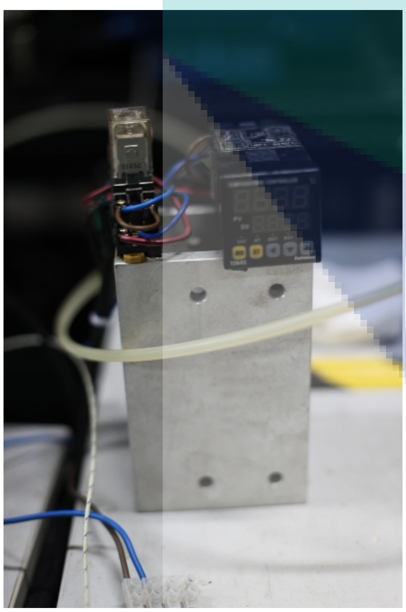

Figure 6 Power supply for the heating source.

2.2.2. Droplet generation/ fuel injection system

Droplet is generated from a direct high-pressure common rail fuel injection system. The fuel injection system was consisting of induction motor, fuel pump, common rail accumulator and fuel injector. Fuel pump with allowable maximum pressure 2000 Bar is connected to the induction motor. The fuel pump is for charging the fuel rail to generate high-pressure fuel. Common rail accumulator is connected to the fuel pump. The high-pressure fuel generated from the fuel pump is fed to the common rail accumulator via high-pressure delivery host. Meanwhile, a low pressure fuel supply host is connected to the fuel tank. Fuel return or excess from the high-pressure fuel pump, rail accumulator and injector are relieved back to the second fuel tank. A high pressure fuel injector with six-hole nozzle and orifice diameter of 0.2 mm each were used to inject the fuel into the optical accessible constant volume chamber. The injector has undergone minor modification from six holes to a single hole. The injector is position at the top of the chamber with approximately 45º incline position to allow nozzle hole to point out straight down for spray penetration proportion to gravity force. Figure shows the tip of the injector inside the chamber. Injector trigger has been set with three-second delays from the click start button.

Figure 7 Tip of the injector inside the chamber

2.2.3. Temperature/ pressure monitoring and control

The pressure transducer and pressure gauge were connected to the common rail accumulator and controlled manually. The pressure sensor was installed on the accumulator common rail with the purpose to control the fuel injection pressure level. The transducer was installed to convert the physical quantity of the pressure detected into an electrical signal. Pressure relief valve with pressure relief passage is installed at the end of the common rail accumulator to control and limit the overbuild up pressure in the system for safety purposes.

Considering the reliability, availability and affordable, thermocouple type K (Nickel-Alumel/ Nickel-Chromium) was chosen and installed to monitor the external chamber temperature. Maximum continuous temperature limit thermocouple type K can handle is 1100°C with accuracy ± 2.2°C or ± 0.75% and special limit of error around ± 1.1˚C or ± 0.4%. The second and similar specification thermocouple was inserted from the fuel injector hole access into the chamber to record the inner chamber temperature before the actual injection.

2.2.4. High-speed camera setup

Video camera trigger was done manually prompt to injection pressure accumulated in the common rail reach the desired reading level. Figure shows the high-speed camera brand Phantom Miro 310/311LC. It has the capability of frame rates up to 650,000 frames per second (fps). However, the speed was compensated by the need to change the trade of time resolution with the sensitivity to the light. For a macroscopic approach, full spray view was visualized using Phantom Miro 310/311LC mounted with AF Micro NIKKOR lens 60 mm f/2.8D. For a strong backlight source, Multi LED LT-V8-15 Tokyo, Japan was used. Software control was Phantom Multicam with 1 μs minimum exposure. White paper sheet was used as backlighting filter. For microscopic view, the same setup was employed with AF Micro NIKKOR lens was replaced by long-distance microscope Infinity-K2 coupled with a zoom lens or known as Objective-CF1 as seen in Figure .

The number of define pixel to capture an image is defined as resolution. For spray study, the resolution setting was set to 128 x 400 pixels at 30,000 fps. For the microscopic study, the resolution was set to 256 x 128 with sample rate at 45, 491 frames per second. Extreme Dynamic Range (EDR) mode is a unique feature of the recent high-speed camera model. The purpose of the feature is to allow each pixel in the frame to receive one or two short exposure time for detected overexposed pixel or slightly longer exposure for the pixel that received normal lights level. The EDR exposure time is set to 0 μs.

With a single-lens reflex camera (SLR), the mirror is positioned in front of the shutter, flip-up, away from the shutter, temporary block viewfinder, shutter move away, exposing light, shutter closed followed by the mirror. In order to overcome the shutter delay, video recording was chosen considering it as the best option. Global shutter is needed to get a better shot of scientific analysis because of the very fast-moving object. Unlike a mechanical shutter that captured each line of pixel one line at a time. In a single image, each pixel is captured gradually or not at the same exact time spot. Thus, the global shutter is the best option. Every single pixel is taken at the same spot of time. The high-speed camera is equipped with a global electronic shutter with minimum exposure of 1 μs. A long exposure gives a bright static image but any motion, the image will be blurred. Short exposure is ideal for motion. Since the motion is very fast, the best practice is to have very bright support light for high shutter speed setting. This is because the exposure duration to light is very short, hence limited light will be captured. As a result, the darker image appeared. In this study, auto exposure was enabled with 0 μs frame delay. For a macroscopic approach, exposure (shutter) time was set between 30 to 40 μs with 0 μs frame delay. For the microscopic approach, exposure was set to 2.02 μs and an auto-exposure was enabled and locked at the trigger.

Phantom Miro 310/311LC operates in 12 bits' mode, hence, the acquisition was set to 12 bits per colour for both approaches. The camera is positioned approximately 50 cm from the centre of the chamber as seen in Figure . Camera pointing at the centre of the tip of the injector installed in the optical constant volume chamber as seen in the Figure . A manual adjustment was done from the injector tip by using adjustable focus located at the lens to obtain sharp images. The optical scale was 0.24 mm/pixel. Similarly, the camera position was adjusted manually to get a sharp view of the image. For both approaches, the recording format was raw CINE. The high-speed camera was powered by using an AC power adapter connected to the computer. Fully spread, stable Tripod with independent extensible leg and spreader was employed to hold and secure the position of the camera. Other mobile mounting was not necessary. To avoid unnecessary camera shaking or an accidental movement due to the manual finger pressing button located at the camera, a remote button trigger was installed.

Underexposure will cause the image too dark while overexposure will cause the image too bright. To avoid any extreme cases while avoiding damaging the camera, auto exposure brackets mode was enabled. For droplet study calibration, a ruler is inserted at the fuel injector mount hole located at the side of a cylindrical constant volume chamber. The ruler was carefully inserted at the centre of the hole that matches the centre of the fuel injector. For spray study, the camera was focally aimed at the ruler as seen in Figure **Error! Reference source not found.**. For droplet study calibration, a similar practice was exercised as seen in Figure . The camera was the first zoom and aim at the injector aiming for texture detail of the nozzle tip. The camera carefully zoomed in and out to focus and reveal the surface roughness nozzle tip. Once the detail is observed, the high-speed camera was carefully tilted up or down and pan left or right to systematically locate the region of the target. It was an extreme close up shot and is suitable for revealing detail.

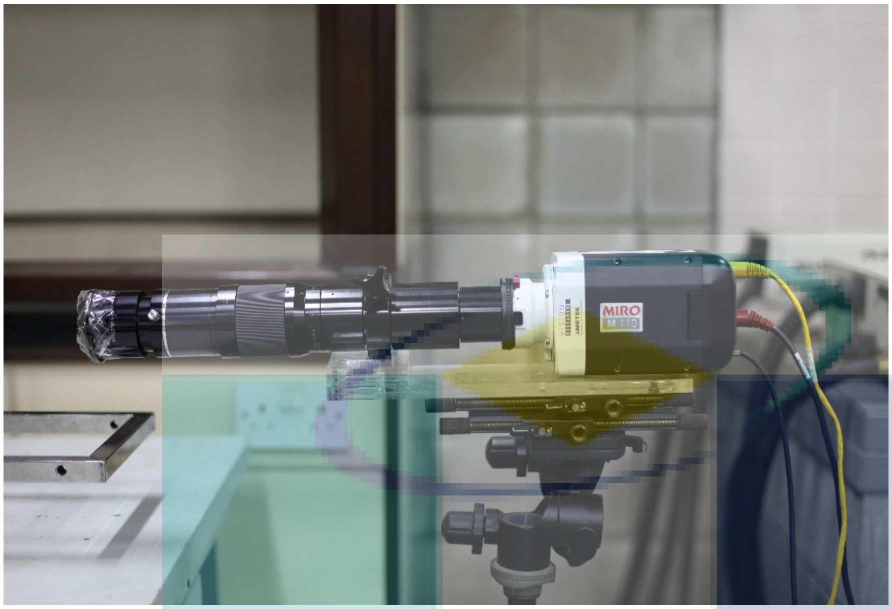

Figure 8	High-speed camera brand Phantom Miro 310/311LC.

Figure 9	Camera pointing at the centre of the tip of the injector installed in the optical constant volume chamber.

Figure 10 Calibration for spray study.

Figure 11 Focus and calibration for droplet study before zoom in.

2.3. Analysing the spray and the micro-explosion phenomenon

The method was adopted from previous studies (Corral-Gómez et al., 2019; Tang, Feng, Zhan, Ma, & Huang, 2017; Zhan et al., 2018). Figure shows the selected definition of spray cone angle and spray penetration adapted from the previous study (Tang et al., 2017). C. Tang et al (2017) measure spray cone by first of all dividing the spray penetration into half and connect the two end spray point of that half. Figure shows the adapted definition of spray spread defined from the measure radial distance.

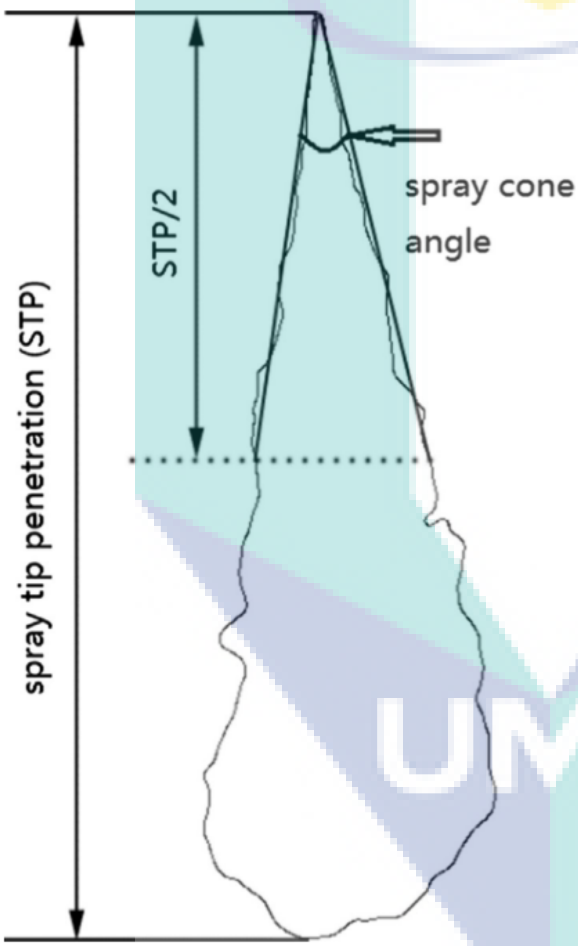

Figure 12 Definition of spray cone and the spray penetration
Source: (Tang et al., 2017)

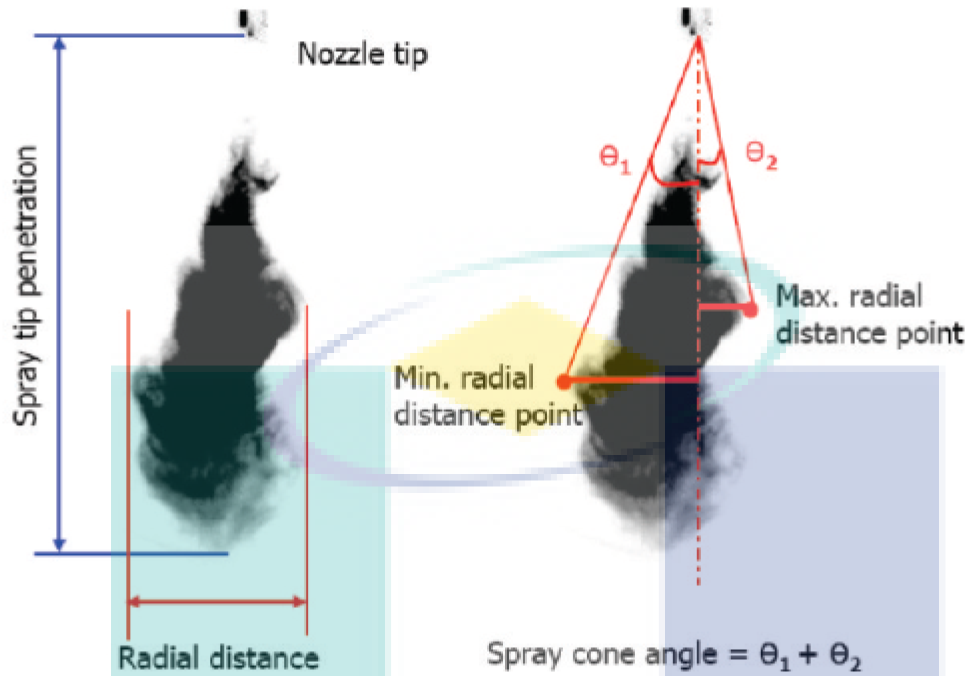

Figure 13 Spray tip penetration and radial distance (mm) and (b) spray cone angle (degrees)

Source: (S. H. Park et al., 2009)

In order to capture the specific event of micro-explosion phenomenon on a single droplet, the camera focus was specifically positioned on a few millimetres after the spray nozzle tip. Instead of targeting only at the left or right side of the spray, the targeted area focuses from the tip of the orifice to further down. The method was adopted from the previous study (Ismael et al., 2018). Meanwhile, to capture the spray characteristics, the camera was positioned horizontally straight line from the spray at a distance of approximately 40 cm from the optical accessible chamber.

2.3.1. Image processing and data analysis technique

Visual motion-captured were exploited in various settings. Visual description of an event was presented with common ground found in all the three selected samples of tri-fuel emulsion. The fascination of the captured event was breakdown into an up-close and personal noted observation. The speed of the droplet breaks up caused by the micro-explosion was expected to be very fast. It could have never been possible to notice and watch with the naked eye without high frame rate capacity of the high-speed camera. The set of a still image is presented to detect static and dynamic feature of micro-explosion phenomenon of tri-fuel emulsion droplet under high-pressure injection in the constant volume chamber at high temperature. In addition, the geometry of the droplet was quantified and plotted. Quantitative analysis procedure involved extracted image from video format and process it as an individual frame with image processing software.

After identifying and selecting the desired frame from the recorded video, The processing of the video was performed by first, converted the video from CINE format to individual sequence static image in Tagged Image File Format (TIFFs). TIFFs save the date in a lossless format. In other words, the data can be saved as 8 or 16 bits over itself repeatedly without losing any single image quality along the road. In comparison to JPEG, TIFFs can store more information with greater quality. Furthermore, TIFFs require no conversion like RAW files. With TIFF format, each of the image frames was processed. Some of the TIFF images require conversion into JPEG format before processing can take place. Then, the image is cropped, sharpened, removed the noise and processed before measurement can be done. Since no image is perfect or absolute noise-free, native noise reduction tool was applied with edge-preserving. Noise reduction filters have three settings; strength, preserve details and reduce colour noise. All the images were processed by using a freely available open-source software called ImageJ.

The image enhancement process is to improve the quality of the image with the help of spatial and frequency domain. Here the type of images that can be converted to digital form. Binary or black and white with an only two-pixel value which is 0 and 1. Grey (0 to 255) and coloured (RGB). 1 element equal to 8 bits. Derived from the spray image using the software, the image was processed for analysis. The processes include edge detection, split colour channel, sharpening, binary, histogram and colour balance. The following step was followed to obtain the data via the build-in ImageJ measuring tool. A similar method was adopted and repeated with a single droplet analysis. The image was derived from the countless selected droplet that undergoes a micro-explosion phenomenon.

Resolution is a dimension of which we can measure how many pixels are on the screen. An image is actually a matric. Grey level is a value of that pixel. Pixel is measured with a special image captured of known measurement such as a ruler. Once calibrated, the pixel can be used to measure the droplet image. Quantification of snapshot concern with calibration for pixel measurement. The pixel aspect ratio was set to 1.0 with known distance as per scale on the ruler; 1 mm. For spray study, the set scale was 4.4638 pixel/mm ± 0.2 pixels/mm while for droplet study the set scale was 37.0539 pixel/mm ± 2 pixels/mm. With the calibrated scale of the pixel setup in place, droplet surface area and axial distance subject to axial direction X or Y of burst out droplet could be measured easily using the processed image. Point to note is that axial distance Y refers to the same direction as the gravity pull. The measured droplet diameter could then be used to calculate the droplet centricity. Spherical status of a droplet can be represented by the droplet centricity which is the ratio of shortest to the longest measured axial distance (droplet diameter) adapted from the previous study (Ghaemi et al., 2008).

2.4. Experimental Method for combustion characteristic investigation

2.4.1. Engine setup

The method was adopted and modified from the previous study (Awad, Mamat, M. Ali, Fahmi Othman, & Abdullah, 2017; A. F. Chen et al., 2018; Kamarulzaman, Abdullah, & Mamat, 2019; Mahmudul, Hagos, Mamat, & Abdullah, 2016; Mahmudul, Hagos, Mamat, Noor, et al., 2017; Musthafa, Kumar, Mohanraj, & Chandramouli, 2018). The experimental work was conducted in the Faculty of Mechanical Engineering, Universiti Malaysia Pahang. A single-cylinder water-cooled horizontal positioned 4-stroked diesel engine was used in the current study. The detail specification of the engine is provided in Table .

Table 2 Engine specification

Description	Specification
Engine Model	YANMAR TF120
Engine Type	Horizontal diesel 4 stroke cycle
Fuel Injection type	Direct injection
No of Cylinder	1
Bore x Stroke	92mm x 96mm
Fuel injection pump	Bosch
Injection timing	17^0 Before Top Dead Center
Displacement (L)	638 cc
Compression ratio	17.7:1
Rated power	9.0 kW at 2400 RPM
Rated Torque	43.35 N.m at 1800 RPM

The setup used was a four-stroke single-cylinder diesel engine model YANMAR TF120. The schematic diagram of the simplify experimental setup is shown Figure .

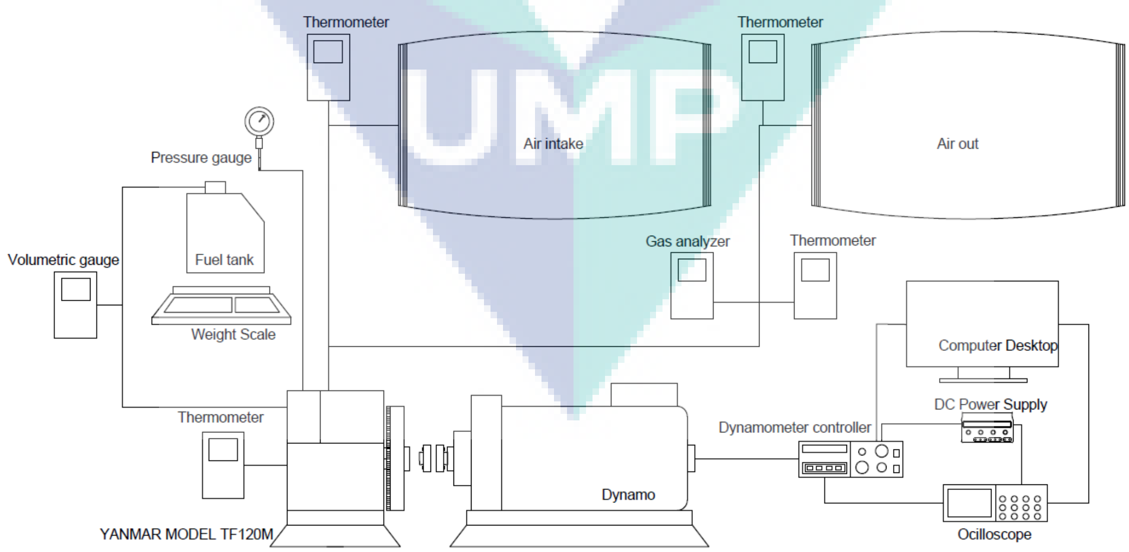

Figure 14 Experimental setup for the investigation of the combustion characteristics

2.4.2. Instrumentation and measurement

The engine was coupled with eddy current dynamometer model BD-15KW from Focus Applied Technologies with maximum electric power capacity up to 15kW. S-type load cell force sensor (Zemic H3-C3-500 Kg-3B) was installed to measure engine brake torque. Hall Effect proximity sensor (AOTORO SC12-20 k proximity sensor, type PNP-NO, M12 4-24VDC, and 20 mA) was installed. It was installed to locate the selected pattern crank trigger sensor plate installed on the dynamo that presenting the position of the top dead centre (TDC). TDC is when the piston at the highest position on the compression stroke. Therefore, the sensor is one of the most important sensors for engine management specifically to determine engine speed and position. There is countless different sort of sensor and crank trigger sensor plate in the market. Type of sensor used and the pattern of the trigger sensor plate was configured within the software. Trigger type, trigger signal and home signal are the common setting in the trigger configuration tab in the software that requires standard professional calibration procedure. DEWESoft X2 software was used as a combustion analyser tool to record resolution at every 0.1^0 CA.

The Optrand fibre optic-based pressure transducer model Auto-PSI C82294-Q was installed to obtain the in-cylinder pressure reading. The cylinder pressure sensor was mounted directly to combustion chamber ranges up to 3000 psi, and sensitivity of approximately 2.63 mV/psi. For analogue to digital signal conversion, data acquisition system was needed. Data acquisition system brand DEWESoft DAQ model SIRIUSi-HS was used. The technology picked up, converted and amplified analogue signals from the pressure transducer sensor and proximity sensor. The system is compatible with Windows and allow simple USB and Ethercat cable connection.

2.4.3. Data analysis

The parameter of interest in the combustion analysis includes heat release rate, in-cylinder temperature and the in-cylinder pressure. IMEP was used as meant to HRR and the in-cylinder temperature was derived from the in-cylinder pressure captured data. HRR was calculated using equation **Error! Reference**

source not found. derived using the first law of thermodynamics for an open system.

$$\frac{dQ}{d\theta} = \frac{\gamma}{\gamma - 1} p \frac{dV}{d\theta} + \frac{1}{\gamma - 1} + V \frac{dp}{d\theta} \qquad 2.5$$

Where:

$\frac{dQ}{d\theta}$ = heat release rate of change with regards to the crank angle change

ϴ = crank angle

$\frac{dP}{d\theta}$ = rate of pressure change in with regards to crank angle

γ = ratio of the specific heat as cp/cv

V = Volume at any crank angle position

Indicated Mean effective pressure (IMEP) which is independent of the engine size and cylinder number was used as a relative selection of performance cycle. IMEP was calculated from the pressure reading collected via the pressure sensor using the equation 2.. Procedure for selecting the cycle which represents the average cycle is as described.

$$IMEP = \frac{\Delta\theta}{Vd} \sum_{i=n1}^{n2} p(i) \frac{dv(i)}{d\theta} \qquad 2.6$$

Where,

IMEP = indicated mean effective pressure

P(i) = in-cylinder pressure at crank angle i

V(i) = in-cylinder volume at crank angle i. n1 and n2 representing two successive BDC crank angle position

The results are defined as the average of three recorded tests run with 200 cycles each. In other words, each sample with an average of 600 cycles per load. Selection of cycle for combustion characteristic processing was done by first extracting all data to excel files. From the first 200 cycles from the first test, the IMEP average was obtained. IMEP average was calculated using equation 2.. Then, Coefficient of variation (COV) IMEP was calculated from the average IMEP as per equation 2 and expressed in percentage. The equation is actually defined as the ratio of the standard deviation of IMEP to the average of IMEP. The standard deviation of IMEP was calculated using equation **Error! Reference source not found.**. Next, from the 200 cycles, the one closest to 0 value was selected. The process for all three tests (600 cycles) for each sample was repeated. The test with the smallest COV IMEP was selected and from that selection of test, one of the cycle within that test with the value closest to the average IMEP was selected. The same procedure was repeated for other samples. Use the same selected cycle in each sample for the next combustion characteristic test

$$IMEP\ average = \frac{1}{n}\sum_i^n p(i)\ IMEPi \qquad 2.7$$

Where:

n = recorded number of the power cycle

$$COV\ IMEP = \frac{\sigma IMEP}{IMEP\ average} \times 100\% \qquad 2.8$$

$$\sigma\ IMEP = \sqrt{\frac{\sum_{i=1}^{n}(IMEP\ average - IMEPi)^2}{n-1}} \qquad 2.9$$

Ignition delay period was derived from the HRR diagram. The delay period was presented from the point of a fuel is injected at 17^0 before TDC. Expected drop of HRR after the point of injection till the HRR increase and cross the horizontal line where the point of injection start.

2.4.4. Procedure and setting

All of the experiments were conducted in the evening with varied ambient temperature ± 33^{0}C and 37^{0}C respectively. The relative humidity level ranged from 80% to 90%. The fuel line was flush out every time the fuel is changed. The engine was left running for a warm-up period at idle speed and zero engine load condition before each actual experiment was executed. The start of fuel injection was fixed at 17˚C before top dead center (BTDC). Load setting was set to 0, 25%, 50%, 75%, 100% representing 0Nm, 7Nm, 14Nm, 21Nm, 28Nm (Newton Meter) respectively. The engine speed was set to constant 1800 RPM ±2. The selection of the speed is based on the optimum brake thermal efficiency suggested in the literature.

The standard operating procedure is as follows:

- Place the fuel jug on the mass weight.
- Switch on the computer.
- Switch on the gas analyser.
- Switch on Dyno controller.
- Switch on the mass weight for fuel consumption.
- Start the engine manually.
- Take full control of the fuel engine throttle manually.
- Connect gas analyser host
- Check all sensor detection display.
- Start the timer and let the engine run for at least 15 minutes.

- Set the desired load and monitor the increase of RPM. Adjust to the desired RPM and desire load by manually adjusting the mechanical throttle.

- Open DynoMon-3 program, PLW recorder program and DEWE Soft X program with setup for Combustion w OPT.

- For PLW recorder, create a file with the name of the fuel_speed_load_and the no of the run. Example: D80E10B10_1800rpm_30percent_run1

- If the fuel consumption is not detected on the software, do it manually. Weight the fuel before and after the run while not to forget the duration run.

- Next, on the DEWE Soft X, press the “store” button and name the new file with a specific file name. Example: D80E10B10_1800rpm_30percent_run1

- Let the engine run and monitor the cycle until it reaches more than 200 cycles.

Collect data

3. LITERATURE REVIEW

Refer the article “Mukhtar, M. N. A., Hagos, F. Y., Noor, M. M., Mamat, R., Abdullah, A. A., & Aziz, A. R. A. (2019). Tri-fuel emulsion with secondary atomization attributes for greener diesel engine–A critical review. *Renewable and Sustainable Energy Reviews*, *111*, 490-506. “ Appendix 1.

4. FINDINGS

4.1. Characterization of the micro-explosion and spray of tri-fuel emulsion

In this section, fuel spray of three different tri-fuel emulsions was investigated for the micro-explosion phenomenon through the use of an optically accessible constant volume chamber and high-speed camera setup as discussed in Chapter 2. The result presentation is classified into two sections namely micro-explosion as secondary atomization characterization and the spray characterization. The micro-explosion as secondary atomization section is further discussed through presentation of the characteristics such as visual motion, droplet surface area change, centricity with minimum and maximum diameter change, axial distance. Furthermore, the spray characterization is presented through subsections of spray cone angle, spray spread on the axial direction and spray penetration.

4.1.1. Micro-explosion and secondary atomization characterization

Micro-explosion phenomenon can occur as high or low intensity with the effect of dynamic structure on a droplet within a relatively short and critical period. It can be seen that the micro-explosion phenomenon for all three samples was identical and have some common dynamic structure. A small scale micro-explosion known as puffing was observed in great detail. This can be explained probably due to the governed effect by the balance between ethanol extreme effect and biodiesel compensation attribute. Specifically, the surface tension and viscosity of tri-fuel emulsion were not as superior as diesel. The biodiesel ratio effect on surface tension may have to prevent the explosion to be a lot more severe. Micro-explosion observed in this study is classified under low-intensity type known as puffing due to high interfacial tension of biodiesel influence and consistent with the reported result on the previous study elsewhere (Qian et al., 2019).

Image processing such as threshold, noise reduction and edge detection plays an important role in distinguishing the effect of micro-explosion phenomenon on a droplet. Figure Error**! No text of specified style in document.**. shows selected zooming raw image sequence of puffing event after threshold and noise removal. The progression of droplet deformation can be seen occurs within a short period. A similar event was captured for all three samples except in pure diesel droplet. Micro-explosion was observed to occur in a variety of size and end up with similar deformity. The micro-explosion phenomenon found was under low-intensity category known as puffing and in this case, the author classified the event as double-side puffing and single side puffing. The classification has not been documented in the previous literature.

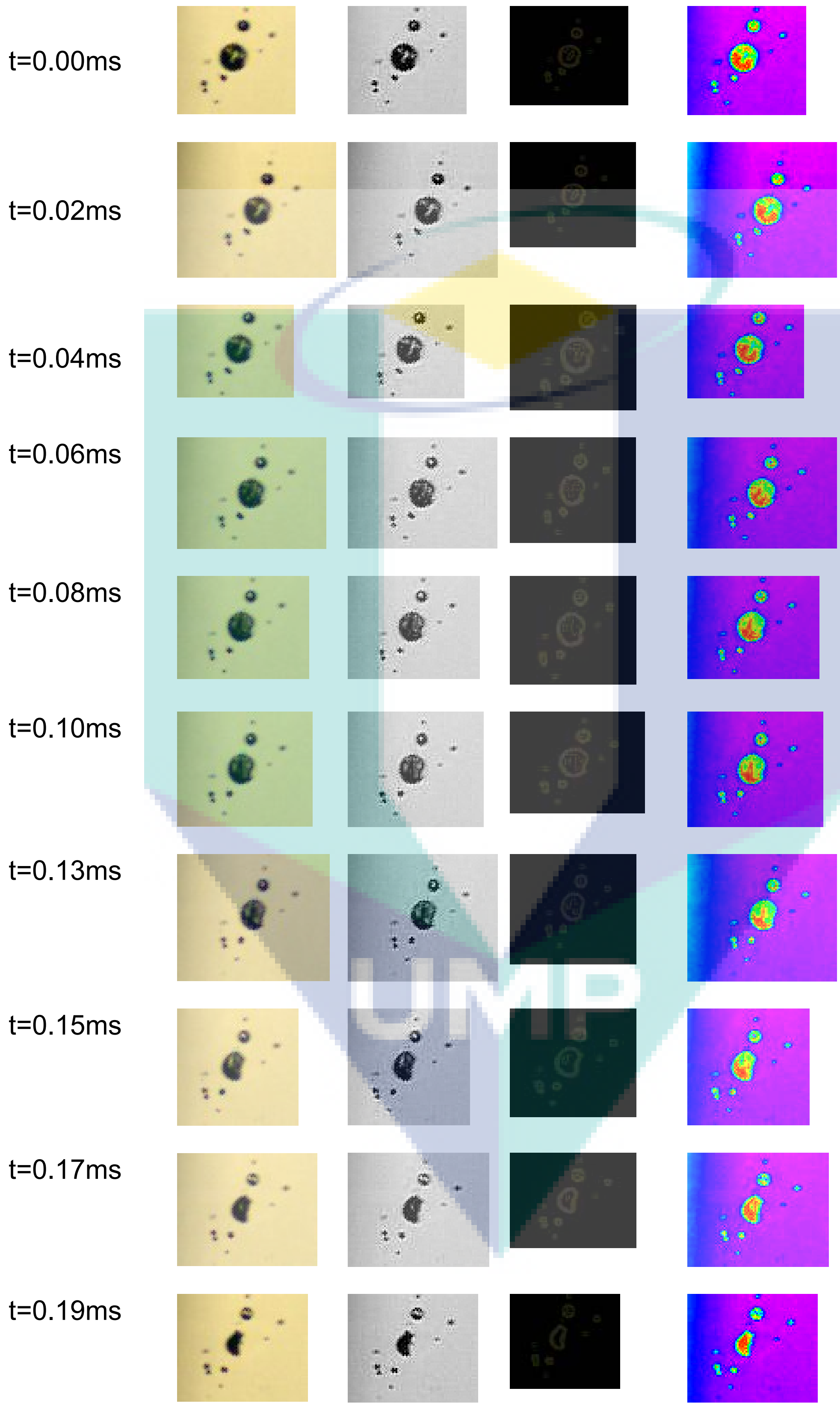
t=0.00ms
t=0.02ms
t=0.04ms
t=0.06ms
t=0.08ms
t=0.10ms
t=0.13ms
t=0.15ms
t=0.17ms
t=0.19ms

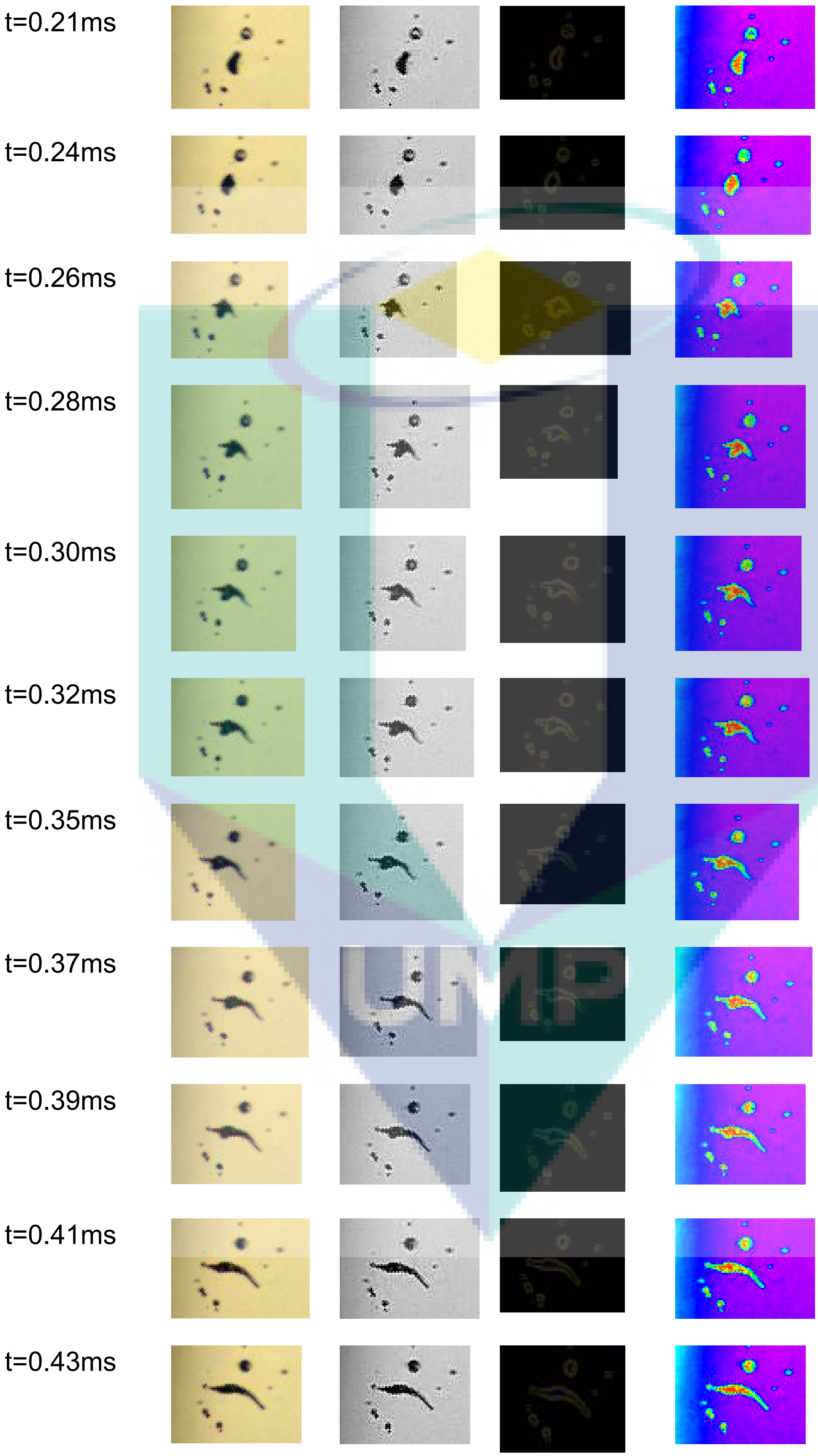
t=0.21ms
t=0.24ms
t=0.26ms
t=0.28ms
t=0.30ms
t=0.32ms
t=0.35ms
t=0.37ms
t=0.39ms
t=0.41ms
t=0.43ms

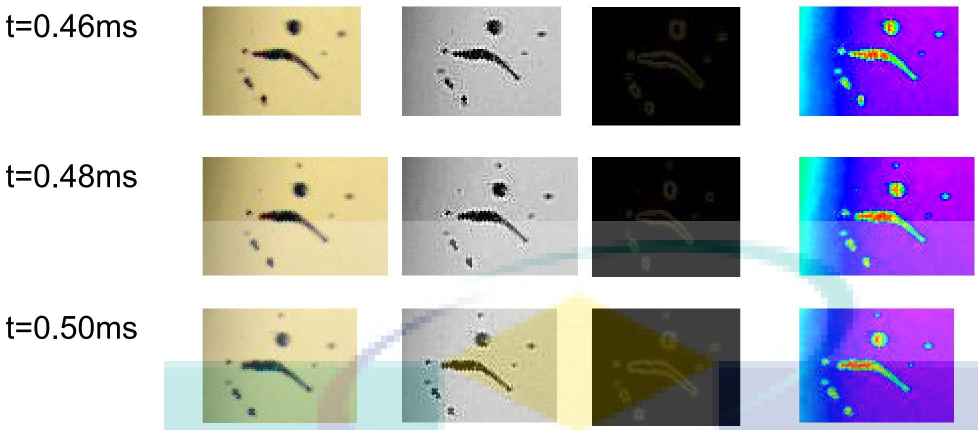

Figure **Error! No text of specified style in document.**.1 Comparison of micro-explosion phenomenon in the form of dual side puffing with time after the fuel injection.

Puffing could also occur as single side puffing. The one side effect of puffing is important to study because it can be considered as half the effect of double-side puffing as described in the previous figure. Figure Error! **No text of specified style in document.**. shows sequence image of single side puffing evolution taken from S20. The puffing was observed to have a significant impact on the droplet during the spray injection. It was observed that the droplet was experiencing a shrinking episode before a unidirectional explosion was recorded. In consequence to the micro-explosion, a recoil effect could be clearly seen to the droplet as it was moving to the opposite direction relative to the explosion.

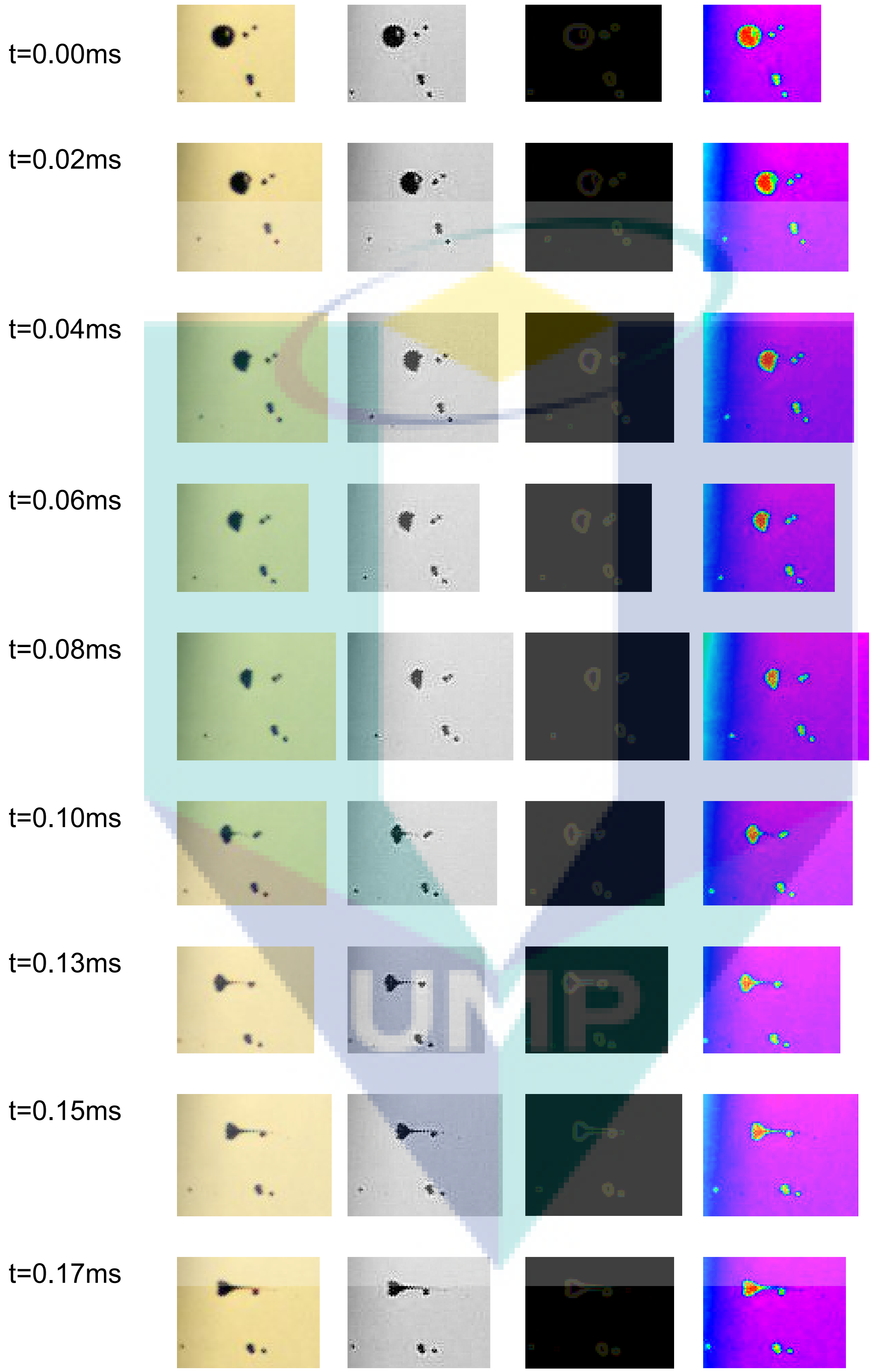
t=0.00ms
t=0.02ms
t=0.04ms
t=0.06ms
t=0.08ms
t=0.10ms
t=0.13ms
t=0.15ms
t=0.17ms

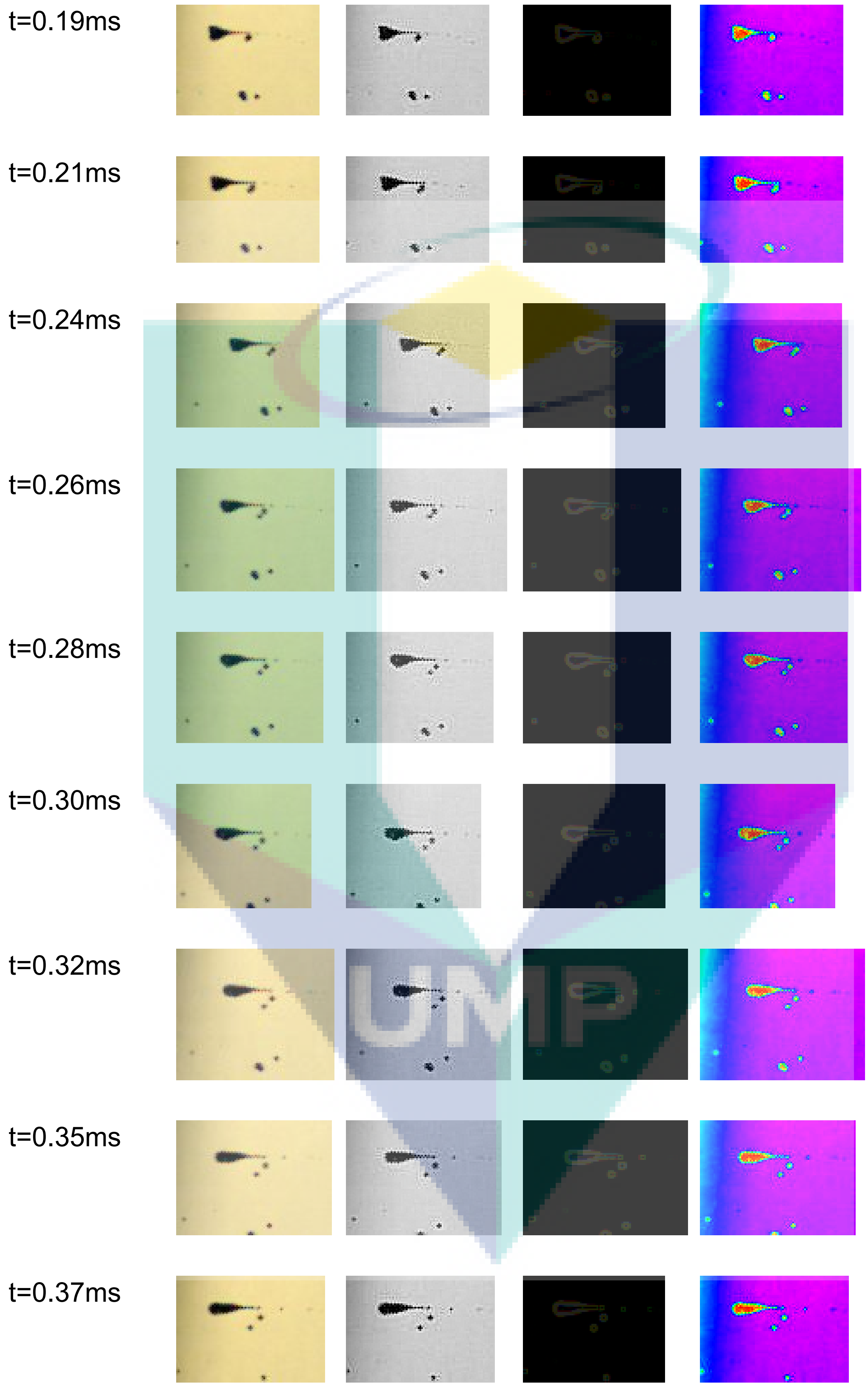
t=0.19ms
t=0.21ms
t=0.24ms
t=0.26ms
t=0.28ms
t=0.30ms
t=0.32ms
t=0.35ms
t=0.37ms

t=0.39ms

t=0.41ms

t=0.43ms

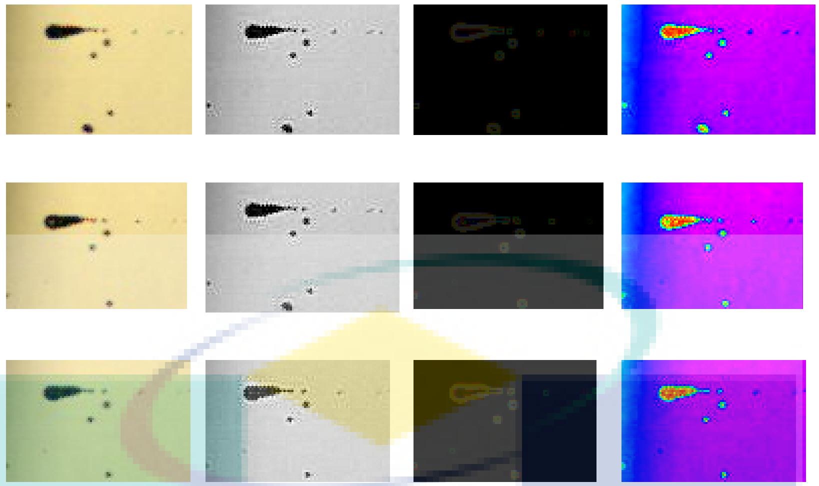

Figure **Error! No text of specified style in document.**.2 Micro-explosion phenomenon in the form of single side puffing with time from the fuel injection

A particularly important sequence noted is from time t=0 ms to t=0.08 ms where the size of the droplet shrinks dramatically before the actual bursting event occurs. This is one of the unusual but frequent behaviours that was observed before the actual eruption in all micro-explosion phenomenon for all three samples. The evolved shape from almost complete sphere shape to almost flat oval shape can be observed in all event of micro-explosion phenomenon recorded. That one moment in time is like all the mass of the droplet is compressed in before been burst out last in a very short amount of time. It sort of closest in for a short period before break apart from the inner core a little moment later. The probable explanation for the droplet diameter is changing bigger and smaller before the explosion because of the boiling occurrence from the inside. The temporary inward compressive force observed was similarly found in the explosion commonly observed underwater. In other words, droplet shrinks to a smaller shape slightly before the micro-explosion phenomenon can be seen in the typical event of a common explosion that occurs underwater (Colicchio, Greco, Brocchini, & Faltinsen, 2015). This event, however, demands another research direction in the future.

In view of the flat oval shape correspond to the final shape after the event, the structure deformation was observed affecting the adjacent droplet and ultimately it may affecting the spray distribution. It can be seen that the almost flat oval shape maintaining its profile for the remaining time unless collide with other droplets nearby. The droplet deformed from spherical shape to oval and eventually to snail figure. The shape like a flying hair has been observed in many spray occasion. The evolution of droplet fragmentation and deformation due to the micro-explosion phenomenon explain this.

Direct evidence obtained that during the event, it was observed that each droplet went through quick phase separation process before micro-explosion starts as stated in the literature review section. This can be distinguished by observing some part of the droplet total dark and the other part with transparency appearance suspected representing the alcohol part. Figure Error**! No text of specified style in document.**. support the discussion with the label part on the droplet with the transparent appearance that represents phase separation that occurs before the micro-explosion phenomenon initiate.

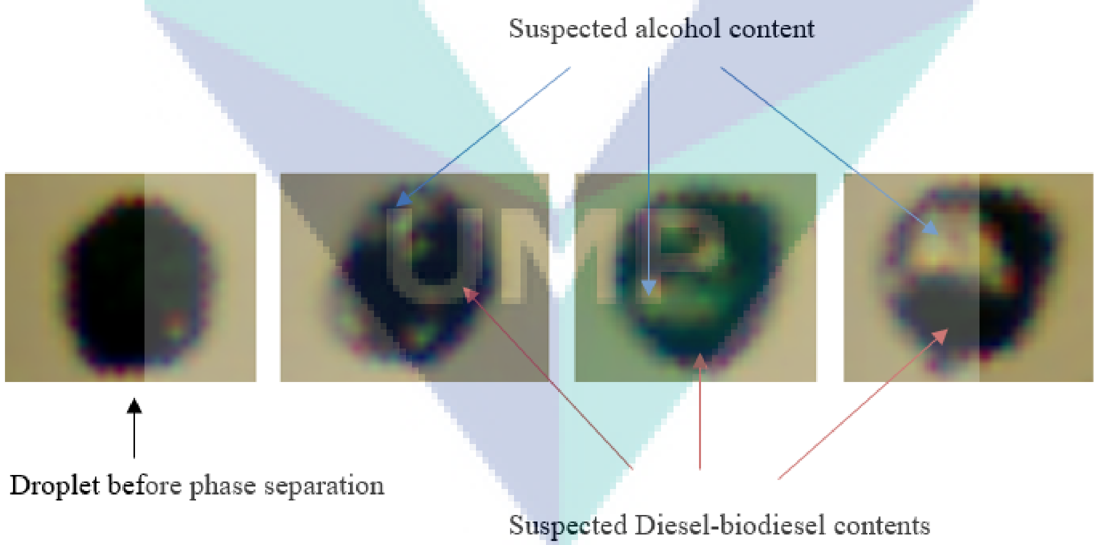

Figure **Error! No text of specified style in document.**.3 Droplet undergone phase separation phase before the micro-explosion phenomenon

It was also observed that the micro-explosion phenomenon causes the droplet to vibrate and bounce a few times before shaping back to the original droplet. The vibration caused by the explosion initiates wavy condition to the original droplet as the droplet came back to its original shape. The vibrated droplet caused by the micro-explosion may or may not change the shape of the droplet. However, in all three samples observed, the effect of the vibration could not exceed the elastic limit of the droplet due to the high surface tension of biodiesel. Hence, the droplet returns to the original shape after multiple time shape transformation. Moreover, the shock wave was release by the micro-explosion observed in the study. The strength and force of the shockwave were not found affecting the surrounding droplet at all direction. However, the momentum of the fragmented droplet shot out of the original droplet did collide with other droplets nearby.

Multiple minor puffing's events were observed to occur at the surface of the droplet in motion. But the occurrence can only be visible with image zoom-in mode. Apparently, the eruption was too small and has no effect on the other droplet nearby. In addition, the eruption has caused the birth of satellite droplets. Meanwhile, at the end of the spray shot under low velocity, micro-explosion phenomenon was observed to occur within the dilatational wave from the process of jet breakup in accordance to the basic theory of basic jet breakup describe by the Raleigh theory and extended by Weber that considered viscosity ("Chapter 10 Atomisation," 2004). Micro-explosion phenomenon was found integrated within the neck formation as a result of oscillation of jet from orifice nozzle.

Micro-explosion reduces the droplet size dramatically. In comparison with droplet undergo normal deformation state, micro-explosion phenomenon deformed the droplet into smaller size or collision with other droplet surroundings. Furthermore, because the droplets were not at constant state and may be affected by the velocity, the droplet collision occurs with other droplets. However, not all collision exercise observed turns out well. In some cases, micro-explosion was seen as common breakup type as described in the theory of droplet atomization process known as shattering. The event of shattering the droplet was captured in Figure Error**! No text of specified style in document.**. Shattering is one of the interesting breakup modes that could possibly occur to a single spherical droplet after subject to relatively sudden impact. However, it was observed in this case, the micro-explosion phenomenon became the ground effect to the droplet undergone the process as a shattering process.

Figure **Error! No text of specified style in document.**.4 Micro-explosion as a shattering process

The micro-explosion phenomenon accelerates the droplet fragmentation process in addition to the influence of velocity caused by the injection pressure and evaporation process caused by the high temperature. This can be explained by referring to the value back to back alcohol and biodiesel with regards to surface tension. Agglomeration that was observed due to vigorous particle collision from the inside of droplet causes the dramatic shape change with time.

Micro-explosion under puffing category that was observed some of them have a common thread. They turn to change shape and got stretch to x-axis direction. Evidently, this causes droplet distance of axial x to dramatically increase. It is possible that this phenomenon is responsible for causing the spray shape to become wider and bigger distance on axial x of the spray apart from possible swirl and turbulence effect. Without collision, it was observed that individual droplet that undergone puffing either single side or dual side category will return back to its original shape due to the strong surface tension caused by the influence of biodiesel ratio that exceeds the compensate ethanol effect.

The shape turns odd from normal circle shape and burst. The burst reaches distance in the axial x-direction. Some turns to baby droplet or sometimes people call satellite droplet. Satellite droplet behaves like a normal droplet. No shaking or boiling behaviour observed on satellite or baby droplet. The observation supports the definition of micro-explosion as coalescence between droplet known as puffing and micro-explosion as sudden evaporation of inner component or bursting of boiling from inside the droplet.

Some of the non-spherical droplets are formed due to the aerodynamic effect. It was observed that none of the droplets in oval shape could perform micro-explosion phenomenon as mentioned in the literature review. Recall from the literature review section, this is probably due to the aerodynamic effect that preventing the event from occurring (W. B. Fu et al., 2002; Mukhtar et al., 2019). The droplet may require additional energy to overcome certain thick capsulated area within the droplet surface. In addition to that, surface tension influence by the biodiesel ratio could have made it even harder to burst.

4.1.2. Droplet Surface area change

The effect of the micro-explosion phenomenon on the droplet surface area is important to the study because it relates to the meant of exposing the maximum surface area of a droplet for fast vapour phase transformation to take place. Figure Error**! No text of specified style in document.**. (a) shows the line graph which illustrates a plot comparison between droplet with and without micro-explosion in term of surface area change with time. It can be seen from the droplet that undergoes micro-explosion showed twice a sudden drop and increase, unlike normal droplet. The droplet surface area dropped dramatically from t=0.1ms to t=0.25ms for double side puffing. The sudden decrease of droplet surface area occurs just a moment before the micro-explosion phenomenon. This is followed by a gradual and continuous increment of the surface area up to 0.3ms. The increment is expected due to the micro-explosion burst so long as there is no collision with any adjacent droplet takes place. Without any collision, it can be seen that the final result of the droplet surface area is still far below the original surface area compared to the surface area at the initial point before micro-explosion starts. The directional of the affected area as the surface area gradually increase and will be presented as the axial deformation plot later. In comparison, without micro-explosion, droplet remains steady with no significant rise or fall pattern. Regardless of single or double side puffing, the sudden swallow in gravitational alike effect before micro-explosion resulted in concave down, decreasing surface area before followed by concave down again but with a gradual increasing surface area. In contrast, it is apparent that was not the case with the normal droplet. It was also observed from the normal droplet behaviour that the evaporation rate is extremely small within such a short recording period. Figure Error**! No text of specified style in document.**.(b) is another micro-explosion event that demonstrates single side puffing with an almost similar pattern. The surface area of droplet undergone puffing decrease dramatically for 0.1 ms before increase significantly for a period of 0.3 ms. The droplet gets back to its normal behaviour after that similar to the normal droplet. To sum up, single side puffing effect on droplet surface area appeared to be similar with double side puffing with sudden and significant concave down pattern which opens up more chances for the evaporation process to concur.

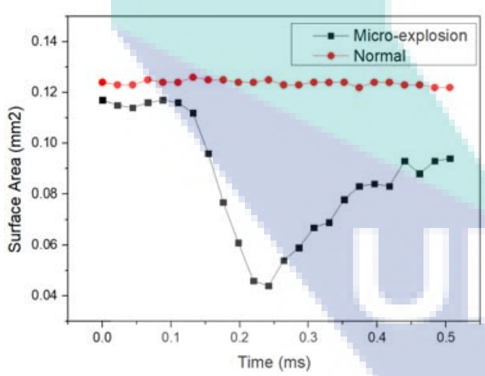

(a)

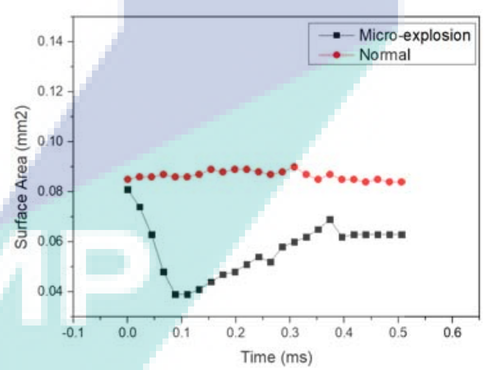

(b)

Figure **Error! No text of specified style in document.**.5 The surface area of droplet undergone (a) double side puffing and (b) single side puffing

The sudden surface area dropped was observed occurs at the initiation stage of the micro-explosion. Evidently, this is because of the initiation of the micro-explosion phenomenon. The finding is important because the surface area decrease of the droplet indicates that the overall atomization process could be improved. Overall, the concave pattern decreasing and increasing is the potential chance for the evaporation process to take place in between the frame. Furthermore, the evaporation rate is extremely small within such a short recording period as observed hence, micro-explosion phenomenon plays its role significantly. The condition of the fuel droplet surface area is determined by how strong is the surface tension. The decrease of droplet surface area may cause the temperature of the droplet to increase and facilitate the evaporation process. The evaporation can take place on the droplet surface. The rate of the evaporation based on the vapour diffusion from the droplet surface.

4.1.3. Centricity with Min and Max diameter change

Droplet centricity represents the spherical status of a droplet. The result is important because it demonstrates the effect of the micro-explosion phenomenon on a droplet in comparison with the normal droplet. Figure Error**! No text of specified style in document.**. (a) shows centricity of droplet undergone double side puffing in comparison with the normal droplet. The value of the droplet centricity was reduced as the droplet going through the event. This indicates that the shape is losing its spherical shape dramatically within a short period. Figure Error**! No text of specified style in document.**. (b) provides information about droplet diameter at the minimum and maximum size in the event of double-side puffing. The information is complimenting in Figure Error**! No text of specified style in document.**. (a). Figure Error**! No text of specified style in document.**. (c) shows centricity of droplet undergone single side puffing in comparison with the normal droplet. The value of the droplet centricity was reduced as the droplet going through the event. Again, this indicates that the shape is losing its spherical shape dramatically within a short period. Figure Error**! No text of specified style in document.**. (d) shows droplet diameter at the minimum and maximum size in the event of single side puffing. It complements Figure Error**! No text of specified style in document.**. (c). The pattern looks similar to double-side puffing.

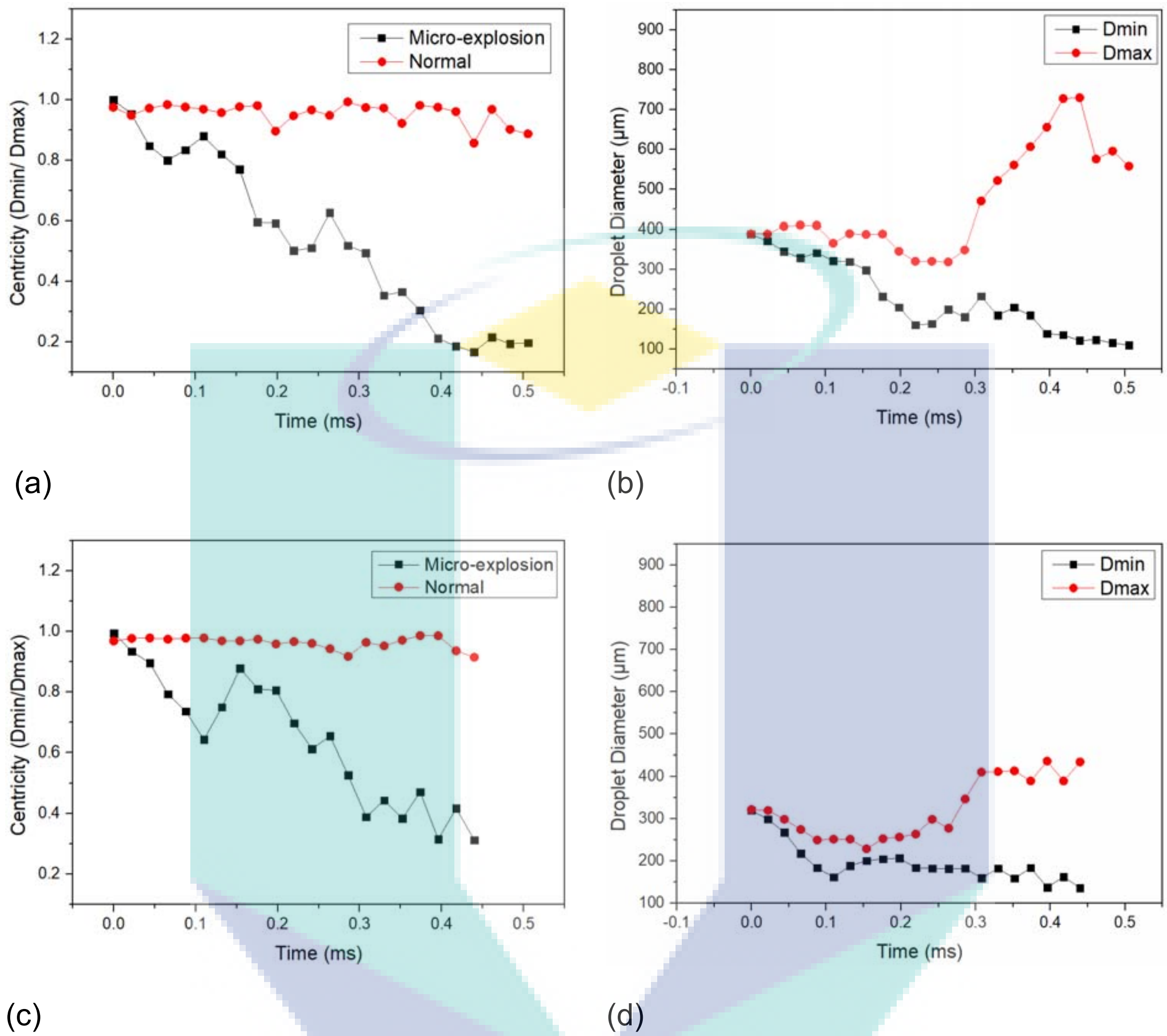

Figure **Error! No text of specified style in document.**.6 Centricity of droplet undergone double side puffing (a) with its droplet diameter (b) and centricity of droplet undergone single side puffing (c) with its droplet diameter

The major finding is that the centricity of the droplet undergone micro-explosion phenomenon decrease significantly within a short period. Regardless of a single side or double side puffing, the centricity of both events shows a similar pattern. The meaning of the finding is that the micro-explosion phenomenon drastically changes the shape of the droplet from common spherical shape to irregular shape subject to the micro-explosion phenomenon. This is not the case with normal droplet behaviour. The finding is important because the sequence of puffing and micro-explosion phenomenon actually affect droplet shape significantly within a short period which could be an advantage to allow the mixing of air and fuel to take place.

4.1.4. Axial distance on X and Y direction

The measured axial distance refers to the distance of the origin droplet and the satellite droplet location as a result of the bursting subject to axial direction X or Y. By analysing the axial distance result subject to the axial direction, one should be able to understand the impact of the phenomenon. Figure Error! **No text of specified style in document.**. (a) shows the effect of double-side puffing on droplet bursting distance on axial x versus time in comparison to a selected droplet of almost similar size without micro-explosion phenomenon. Axial distance X decreased slightly before actual bursting and accelerate the increased of axial distance X. This was not the case with normal droplet behaviour. Figure Error! **No text of specified style in document.**. (b) shows the effect of single-side puffing on droplet bursting distance on axial X versus time. The impact of the burst originated by the micro-explosion was illustrated by the dramatic increase of the axial distance X. For single side puffing, it was observed that the axial distance decreases slightly less than double side puffing at the beginning before accelerate to a positive value significantly after that. Figure Error! **No text of specified style in document.**. (c) shows droplet bursting distance on axial-Y versus time. The droplet with a micro-explosion phenomenon experience a slight decrease in axial distance effect on axis Y in contrast to the normal droplet. The effect however temporary the droplet reshapes and get back to the axial distance original track. Normal droplet did not experience the axial distance change at all within that short period. Figure Error! **No text of specified style in document.**. (d) illustrates droplet bursting distance on axial Y with time due to puffing in comparison with axial distance Y for the normal droplet. Again, the axial distance Y decrease slightly in comparison with the normal droplet. However not as dramatically as axial distance X.

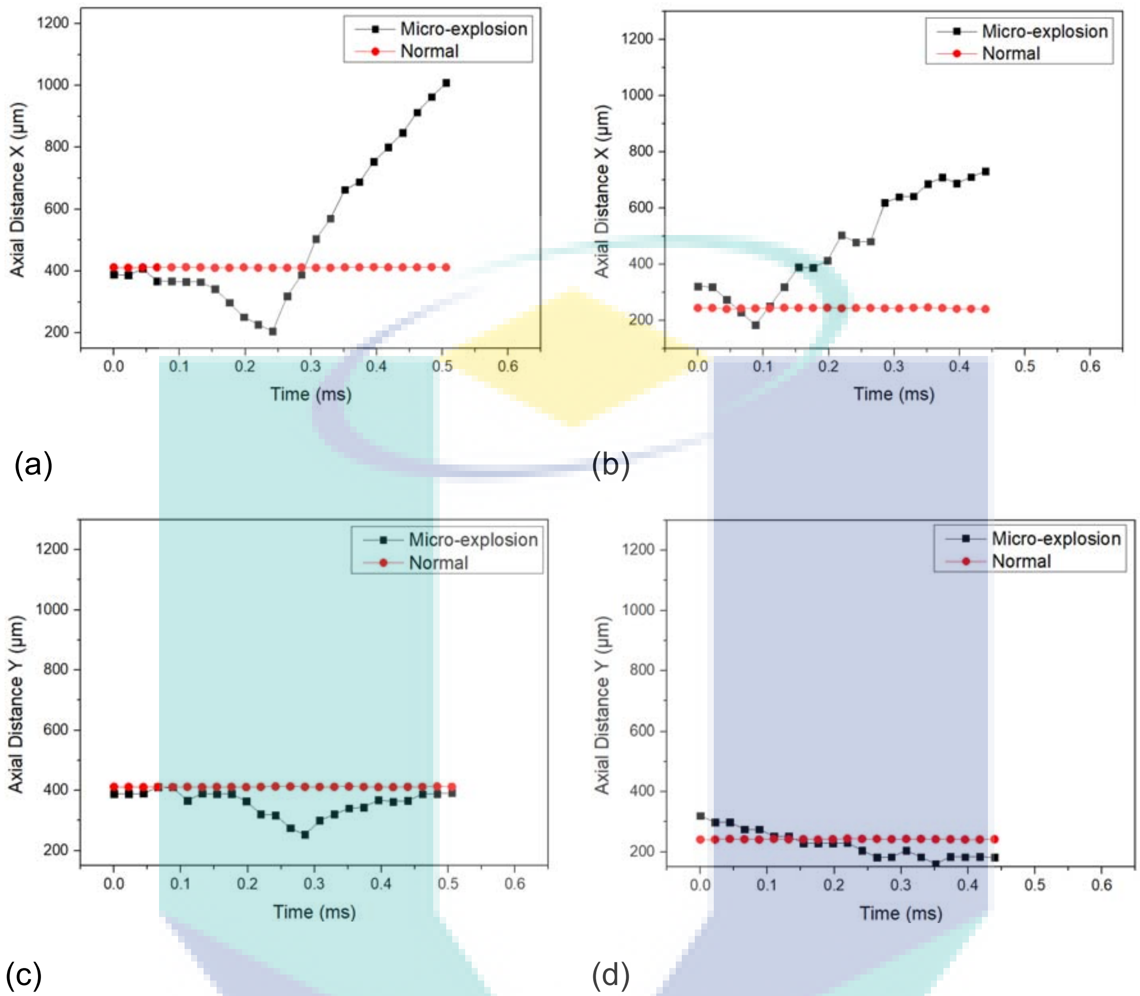

Figure **Error! No text of specified style in document.**.7 Axial distance X of droplet undergone (a) double side puffing and (b) single side puffing. Axial distance Y of droplet undergone (c) double side puffing and (d) single side puffing

The key observation from this experiment is the droplet spreading dynamic causes by low-intensity micro-explosion phenomenon known as puffing. Regardless of single or dual side puffing, the event promotes efficient atomization progression. Within a short period, the finding of micro-explosion impact on the axial distance X of droplet changes significantly different than the normal droplet. The deformation and bursting outcome on axial distance X effect for a single or dual side puffing produce a similar pattern. This is not the case with the effect on axial Y direction. Possibly the effect on axial Y direction yields concaves up pattern because of the surface tension effect as well as the momentum and gravity pull. Furthermore, the impact on axial Y direction which is in the same direction as spray penetration not as much as the axial distance X which is parallel to the spray spread. The meaning of the finding is that the micro-explosion phenomenon affects droplet axial distance X significantly and Y slightly. The event can be considered as a premonition to the spray characteristics which points out that the axial distance formation to the axial X direction and this may one of the explanation of why the spray axial distance increase. The result of the spray spread will be presented and discussed next.

Results on the physicochemical characteristics can be found on published paper in Appendix 2.

5. CONCLUSION

The experiments conducted to achieve the first objective answer the first research question. For objective 1, fuel characterization was the goal and the objective is fully met. Because ethanol and diesel are known to be immiscible in nature, proper biodiesel is included as a stabilizer and require adequate agitation method. Normal agitator such as stirring or shaking may not work and concur fast phase separation. Therefore, the effect of proportion ratio and ultrasonic emulsifying setting on the physicochemical properties of tri-fuel emulsion have been explored. Statistical analysis was done to reveal the interaction between control factors related to agitation mechanisms such as amplitude and cycle as well as control factors related to formulation ratios such as percentage content of ethanol and biodiesel. It was found that the Interaction between control factors exist and affect the physicochemical properties of the tri-fuel emulsion prepared. Density, viscosity and surface tension are the significant properties relevant to the fuel atomization process. Furthermore, droplet quality before and after going through the fuel injection system that previously merely presumed to be identical have been compared. Morphology basis of tri-fuel emulsion droplet before and after the injection has been confirmed. From a number of experiments conducted, the conclusion is made to justify meeting the first objective as follow:

- Percentage of ethanol content has a significant effect on tri-fuel emulsion physicochemical properties without any significant interaction with other control factors.

- Two control factor interaction, mainly ethanol and biodiesel were detected statistically on the viscosity reading.

- Ethanol influence strongly the viscosity and the significant decrease due to the ethanol effect can be compensated by biodiesel opposite effect. In other words, the percentage of biodiesel content compensates for the effect of ethanol.

- Cycle setting plays a significant role to balance the gravity of the interaction between biodiesel and ethanol effect on viscosity.

- Interaction between cycle setting and ethanol percentage on the decrease of surface tension was statistically significant.

- From the interaction between ethanol and cycle setting, with moderate amplitude and biodiesel content, the surface tension dramatically decreased as ethanol increase.

- High cycle setting deescalates the decrease of the surface tension as more ethanol content is added.

- Cross-section interaction between biodiesel and amplitude setting which influence the surface tension outcome is present.

- Amplitude plays a significant role in manipulating biodiesel effect on the increase or decrease of the surface tension.

- Surface tension response oppositely to the high content of biodiesel regardless of amplitude level.

Low or high amplitude with a low percentage of biodiesel resulted in no major difference to the average droplet size. However, with high biodiesel percentage, low amplitude setting contributed to a bigger size, while a high amplitude setting led to more refine size.

100 days' stability test of tri-fuel emulsion revealed three distinct stages of phase separation process timeline. This answer why exists vague of information from the previous study related to tri-fuel stability.

From morphology study, aerodynamic formation due to aerodynamic effect, the location of the dispersed component in the droplet may change, resulting in oval shape droplets formation detected.

In the second objective, the investigation of tri-fuel emulsion undergone micro-explosion phenomenon was executed. Low-intensity category of micro-explosion phenomenon with a single side and double side puffing were observed in great detail. The impact of the micro-explosion has been revealed by the thorough investigation on a located focus image of a single droplet deformation was undergone high-pressure injection. The image of droplet undergone micro-explosion phenomenon was located, processed and quantified by obtaining the diameter, centricity change, axial X and Y spread and the surface area change. Furthermore, high-pressure spray characteristics of tri-fuel emulsion under low and high temperature were compared namely spray cone angle, spray spread – axial distance and spray penetration. The following conclusion is drawn to meeting the second objective of the research: -

- The micro-explosion observed in this study is classified under low-intensity type known as puffing due to high interfacial tension of biodiesel influence.
- The micro-explosion phenomenon accelerates the droplet fragmentation process in addition to the influence of velocity caused by the injection pressure and evaporation process caused by the high temperature.
- Without collision, an individual droplet that undergone puffing either single side or dual side category will return back to its original shape due to the strong surface tension caused by the influence of biodiesel ratio that exceeds the compensate ethanol effect.
- Puffing causes droplet distance of axial x to dramatically increase and possible that this phenomenon that may cause the spray shape

to become wider and bigger distance on axial x of the spray apart from possible swirl and turbulence effect.

- Droplet diameter is changing bigger and smaller before the explosion because of the boiling occurrence from the inside.
- The droplet shape turns odd from normal circle shape and burst reaching distance in the axial x-direction as satellite droplet.
- None of the droplets in oval shape could perform micro-explosion due to the aerodynamic effect that could have to prevent the event from occurring. The droplet may require additional energy to overcome certain thick capsulated area within the droplet surface. In addition to that, surface tension influence by the biodiesel ratio made it even harder to burst.
- Phase separation occurred shortly before micro-explosion initiated indicates that this may be a good indicator for micro-explosion to occur.
- The sudden surface area dropped was observed occurs at the initiation stage of the micro-explosion and not after the micro-explosion phenomenon.
- Overall, the concave pattern decreasing and increasing is the potential chance for the evaporation process to take place in between the frame.
- The centricity of the droplet underwent micro-explosion phenomenon decrease significantly within a short period.
- Regardless of a single side or double side puffing, the centricity of both graphs shows a similar pattern.

- The micro-explosion phenomenon drastically changes the shape of the droplet from common spherical shape to irregular shape subject to the micro-explosion phenomenon.

- The axial distance X effect for a single or dual side puffing yield a similar pattern.

- The effect on axial Y direction yields unique and repetitive concave up pattern.

- The micro-explosion phenomenon affects droplet axial distance X and Y significantly.

- The presence of liquid core during initial injection and short liquid sheet at the end of the injection were observed.

- The effect of the high ambient temperature led to a noticeable spray shape pattern.

- The finding from a spray cone angle suggests that tri-fuel emulsions improvement could be achieved and noticeable only at the beginning of the spray.

- From a radial distance or spray spread plotted under high temperature, significant spray spread improvement was observed for tri-fuel emulsion

- Spray penetration finding suggests that the accumulative droplet within the spray injection causing the momentum of the spray to increase.

The objective is fully met and the finding removed the positional ambiguity of the micro-explosion phenomenon possible occurrence in CI engine. A most important finding from the second objective is the complexity of the breakup process caused by the micro-explosion phenomenon. It was previously not yet fully understood and now in the spotlight. The common structure of droplet gone through micro-explosion phenomenon that is previously unknown has been revealed. Hair look-alike droplet as finding has been interpreted. From origin spherical shape to hair look alike droplet has been discovered.

In the third objective, combustion characteristics of the tri-fuel emulsion were revealed specifically focus on the ignition delay period. Result from single cylinder CI engine test, heat release rate, in-cylinder pressure and in-cylinder temperature were analysed. The following conclusion is drawn to justify meeting the research objective 3:

- Overall ignition delay period comparison with different loads suggest that tri-fuel emulsions require additional time to ignite compared to diesel.

- During the ignition delay period, HRR curve exhibit negative value was due to atomization and evaporation effect

- With 0% load, during the ignition delay period, HRR of tri-fuel emulsion, specifically S17 compete with diesel.

- With 0% load, peak HRR of tri-fuel emulsion specifically S17 was the highest exceeding diesel.

- With 0% load, in-cylinder temperature for all tri-fuel emulsions during the ignition delay period exceed diesel.

- Another significant difference during the ignition delay period was that all tri-fuel emulsions cool down slightly before actual ignition as a result of latent heat of evaporation effect and it was not the case with diesel.

- With 0% load, peak in-cylinder temperature for specifically tri-fuel emulsion S17 was the highest and exceed diesel.

- With 0% load, in-cylinder pressure for all tri-fuel emulsions during the ignition delay period exceed diesel.
- With 0% load, peak in-cylinder pressure for all tri-fuel emulsions exceeds diesel with S17 the highest.
- Load shortening tri-fuel emulsion ignition delay period.

ACHIEVEMENT

i) Name of articles/ manuscripts/ books published

Mukhtar, M. N. A., Hagos, F. Y., Noor, M. M., Mamat, R., Abdullah, A. A., & Aziz, A. R. A. (2019). Tri-fuel emulsion with secondary atomization attributes for greener diesel engine–A critical review. *Renewable and Sustainable Energy Reviews*, *111*, 490-506.

NA, M. M., Aziz, A., Rashid, A., Hagos, F. Y., Noor, M. M., Kadirgama, K., ... & Abdullah, A. A. (2019). The influence of formulation ratio and emulsifying settings on tri-fuel (Diesel–Ethanol–Biodiesel) emulsion properties. *Energies*, *12*(9), 1708.

Awad, O. I., Mamat, R., Ibrahim, T. K., Hagos, F. Y., Noor, M. M., Yusri, I. M., & Leman, A. M. (2017). Calorific value enhancement of fusel oil by moisture removal and its effect on the performance and combustion of a spark ignition engine. *Energy conversion and management*, *137*, 86-96.

Hagos, Ftwi Yohaness, A. Rashid A. Aziz, Shaharin A. Sulaiman, and Rizalman Mamat. "Effect of fuel injection timing of hydrogen rich syngas augmented with methane in direct-injection spark-ignition engine." *international journal of hydrogen energy* 42, no. 37 (2017): 23846-23855.

Hagos, F. Y., Ali, O. M., Mamat, R., & Abdullah, A. A. (2017). Effect of emulsification and blending on the oxygenation and substitution of diesel fuel for compression ignition engine. *Renewable and Sustainable Energy Reviews*, *75*, 1281-1294.

Mahmudul, H. M., Hagos, F. Y., Mamat, R., Adam, A. A., Ishak, W. F. W., & Alenezi, R. (2017). Production, characterization and performance of biodiesel as an alternative fuel in diesel engines–A review. *Renewable and Sustainable Energy Reviews*, *72*, 497-509.

ii) Title of Paper presentations (international/ local)

Bahrudin, M. N. H., Hagos, F. Y., Mamat, R., Abdullah, A. A., & Karim, Z. A. A. (2019, January). Comparison between tri-fuel (diesel-ethanol-biodiesel) emulsion with and without surfactant. In *AIP Conference Proceedings* (Vol. 2059, No. 1, p. 020056). AIP Publishing.

Hassan, M. M., Hagos, F. Y., & Mamat, R. (2018, June). Comparative Analysis of Diesel, Diesel-Palm Biodiesel and Diesel-Biodiesel-Butanol Blends in Diesel Engine. In *ASME 2018 12th International Conference on Energy Sustainability collocated with the ASME*

2018 Power Conference and the ASME 2018 Nuclear Forum (pp. V001T04A007-V001T04A007). American Society of Mechanical Engineers.

Low, M. H., Mukhtar, N. A. M., Hagos, F. Y., & Noor, M. M. (2017, October). Tri-fuel (diesel-biodiesel-ethanol) emulsion characterization, stability and the corrosion effect. In *IOP Conference Series: Materials Science and Engineering* (Vol. 257, No. 1, p. 012082). IOP Publishing.

Lee, K. H., Mukhtar, N. A. M., Hagos, F. Y., & Noor, M. M. (2017, October). A study of the stabilities, microstructures and fuel characteristics of tri-fuel (diesel-biodiesel-ethanol) using various fuel preparation methods. In *IOP Conference Series: Materials Science and Engineering* (Vol. 257, No. 1, p. 012077). IOP Publishing.

iii) Human Capital Development

HUMAN CAPITAL DEVELOPMENT					
Human Capital	**Number**				**Others** (please specify)
	On-going		**Graduated**		
Citizen	Malaysian	Non Malaysian	Malaysian	Non Malaysian	
No. PHD STUDENT	2				
Student Fullname: IC / Passport No: Student ID:	MUHAMMAD MUKHTAR BIN NOOR AWALLUDIN 810821015539 PMM16009 ANUSUIAH VASU 680507755026 16007				
No. MASTER STUDENT				1	
Student Fullname: IC / Passport No: Student ID:				Md. Mahmudul Hassan BB0042730 MMM14046	
No. UNDERGRADUATE STUDENT			5	1	
Student Fullname: IC / Passport No: Student ID:			Muhammad Adzmir Bin Kamaruddin (MA13056) Siti Sabariah binti Muhammad (HB12017) Lee Kar	**Abdulwahid Omar Mohammed Arman** **(MA13212)**	

			Huan (MH13037) Low Ming Hui (MH13040)		
Total	2		5	2	

iv) Awards/ Others

Tajuk Anugerah *(Awards Title)*	**Tarikh/Tahun** *(Date/Year)*	**Penganjur Penganugerahan** *(Organizer)*	***Peringkat** *(Level)*
Silver Medal, Title: TRI-FUEL BASED MICRO-EXPLOSION FOR CLEAN COMBUSTION, 30th International Invention & Innovation Exhibition 2018 (ITEX 2019), Kuala Lumpur Convention centre, Malaysia	02-04 May, 2019	ITEX	National
Gold Medal and special award, Title: Emission reduction through micro-explosion occurrence in tri-fuel combustion", Creation, Innovation, Technology & Research Exposition (CITREX) 2019	12-13 February 2019	UMP	UMP
Gold Medal, Title: Environmental friendly tri-fuel emulsion, 29th International Invention & Innovation Exhibition 2018 (ITEX 2018), Kuala Lumpur Convention centre, Malaysia	10-12 May, 2018	ITEX	National
Gold Medal and special award, Title: Tri-fuel emulsion. A novel method for the stability of tri-fuel emulsion", Creation, Innovation, Technology & Research Exposition (CITREX) 2018, Main Hall, UMP, Malaysia	March 2018	UMP	UMP
Bronze Medal (2017), Tri-fuel emulsion as environmental friendly alternative fuel 2017, indoor stadium complex localized at Kuala Nerus,	7th-9th October 2017	International Conference and Exposition on Inventions by Institutions of Higher Learning (PECIPTA)	National
Gold Medal and special award, Title: Tri-fuel emulsion. A novel fuel for CI engine", Creation, Innovation, Technology & Research Exposition (CITREX) 2017, Main Hall, UMP,	March 2017	UMP	UMP

Malaysia			

v) Others

Intellectual Property

2017001318

Method of identifying emulsifier parameters on stability and preparing stabilized emulsifier for fuel mixture Application: Filed on 22/08/2017

REFERENCES

[1] Bacha J, Freel J, Gibbs A, Gibbs L, Hemighaus G, Hoekman K, et al. Diesel Fuels Technical Review. Chevron Glob Mark 2007:1–116. doi:10.1063/1.3575169.

[2] Reşitoǩlu IA, Altinişik K, Keskin A. The pollutant emissions from diesel-engine vehicles and exhaust aftertreatment systems. Clean Technol Environ Policy 2015;17:15–27. doi:10.1007/s10098-014-0793-9.

[3] Khalife E, Tabatabaei M, Demirbas A, Aghbashlo M. Impacts of additives on performance and emission characteristics of diesel engines during steady state operation. Prog Energy Combust Sci 2017;59:32–78. doi:10.1016/j.pecs.2016.10.001.

[4] Alptekin E. Emission, injection and combustion characteristics of biodiesel and oxygenated fuel blends in a common rail diesel engine. Energy 2017;119:44–52. doi:10.1016/j.energy.2016.12.069.

[5] Tan YH, Abdullah MO, Nolasco-Hipolito C, Zauzi NSA, Abdullah GW. Engine performance and emissions characteristics of a diesel engine fueled with diesel-biodiesel-bioethanol emulsions. Energy Convers Manag 2017;132:54–64. doi:10.1016/j.enconman.2016.11.013.

[6] Arbab MI, Masjuki HH, Varman M, Kalam MA, Imtenan S, Sajjad H. Fuel properties, engine performance and emission characteristic of common biodiesels as a renewable and sustainable source of fuel. Renew Sustain Energy Rev 2013;22:133–47. doi:10.1016/j.rser.2013.01.046.

[7] Hagos FY, Aziz ARA, Tan IM. Water-in-diesel emulsion and its micro-explosion phenomenon-review. 2011 IEEE 3rd Int Conf Commun Softw Networks, ICCSN 2011 2011:314–8. doi:10.1109/ICCSN.2011.6014903.

[8] Moussa O, Tarlet D, Massoli P, Bellettre J. Parametric study of the micro-explosion occurrence of W/O emulsions. Int J Therm Sci 2018;133:90–7. doi:10.1016/j.ijthermalsci.2018.07.016.

[9] Chen Z, Wang X, Pei Y, Zhang C, Xiao M, He J. Experimental investigation of the performance and emissions of diesel engines by a novel emulsified diesel fuel. Energy Convers Manag 2015;95:334–41. doi:10.1016/j.enconman.2015.02.016.

[10] Ooi JB, Ismail HM, Swamy V, Wang X, Swain AK, Rajanren JR. Graphite Oxide Nanoparticle as a Diesel Fuel Additive for Cleaner Emissions and Lower Fuel Consumption. Energy and Fuels 2016;30:1341–53. doi:10.1021/acs.energyfuels.5b02162.
[11] Hansen AC, Zhang Q, Lyne PWL. Ethanol-diesel fuel blends - A review. Bioresour Technol 2005;96:277–85. doi:10.1016/j.biortech.2004.04.007.
[12] Han K, Yang B, Zhao C, Fu G, Ma X, Song G. Experimental study on evaporation characteristics of ethanol-diesel blend fuel droplet. Exp Therm Fluid Sci 2016;70:381–8. doi:10.1016/j.expthermflusci.2015.10.001.
[13] Road XW. Microexplosion of Three-Phase Diesel-Methanol-Water Emulsion Spray 2012;24:2100–6.
[14] Datta A, Palit S, Mandal BK. An experimental study on the performance and emission characteristics of a CI engine fuelled with Jatropha biodiesel and its blends with diesel. J Mech Sci Technol 2014;28:1961–6. doi:10.1007/s12206-014-0344-7.
[15] Abu-Hamdeh NH, Alnefaie KA. A comparative study of almond and palm oils as two bio-diesel fuels for diesel engine in terms of emissions and performance. Fuel 2015;150:318–24. doi:10.1016/j.fuel.2015.02.040.
[16] Mofijur M, Rasul MG, Hyde J, Azad AK, Mamat R, Bhuiya MMK. Role of biofuel and their binary (diesel-biodiesel) and ternary (ethanol-biodiesel-diesel) blends on internal combustion engines emission reduction. Renew Sustain Energy Rev 2016;53:265–78. doi:10.1016/j.rser.2015.08.046.
[17] Shahir SA, Masjuki HH, Kalam MA, Imran A, Fattah IMR, Sanjid A. Feasibility of diesel-biodiesel-ethanol/bioethanol blend as existing CI engine fuel: An assessment of properties, material compatibility, safety and combustion. Renew Sustain Energy Rev 2014;32:379–95. doi:10.1016/j.rser.2014.01.029.
[18] Abedin MJ, Imran A, Masjuki HH, Kalam MA, Shahir SA, Varman M, et al. An overview on comparative engine performance and emission characteristics of different techniques involved in diesel engine as dual-fuel engine operation. Renew Sustain Energy Rev 2016;60:306–16. doi:10.1016/j.rser.2016.01.118.
[19] Pang X, Mu Y, Yuan J, He H. Carbonyls emission from ethanol-blended gasoline and biodiesel-ethanol-diesel used in engines. Atmos Environ 2008;42:1349–58. doi:10.1016/j.atmosenv.2007.10.075.
[20] Xiaoyan SHI, Yunbo YU, Hong HE, Shijin S, Hongyi D, Rulong LI. Combination of biodiesel-ethanol-diesel fuel blend and SCR catalyst assembly to reduce emissions from a heavy-duty diesel engine 2008;20:177–82.
[21] Qi DH, Chen H, Geng LM, Bian YZ, Ren XC. Performance and combustion characteristics of biodiesel-diesel-methanol blend fuelled engine. Appl Energy 2010;87:1679–86. doi:10.1016/j.apenergy.2009.10.016.
[22] Barabás I, Todoru A, Bldean D. Performance and emission characteristics of an CI engine fueled with diesel-biodiesel-bioethanol blends. Fuel 2010;89:3827–32. doi:10.1016/j.fuel.2010.07.011.
[23] Hulwan DB, Joshi S V. Performance, emission and combustion characteristic of a multicylinder DI diesel engine running on diesel-ethanol-biodiesel blends of high ethanol content. Appl Energy 2011;88:5042–55.

doi:10.1016/j.apenergy.2011.07.008.
[24] Pidol L, Lecointe B, Starck L, Jeuland N. Ethanol-biodiesel-Diesel fuel blends: Performances and emissions in conventional Diesel and advanced Low Temperature Combustions. Fuel 2012;93:329–38. doi:10.1016/j.fuel.2011.09.008.
[25] Labeckas G, Slavinskas S, Mažeika M. The effect of ethanol-diesel-biodiesel blends on combustion, performance and emissions of a direct injection diesel engine. Energy Convers Manag 2014;79:698–720. doi:10.1016/j.enconman.2013.12.064.
[26] Mahmudul HM, Hagos FY, Mamat R, Abdullah AA, Awad OI. Experimental investigation of the impact of using alcohol- biodiesel-diesel blending fuel on combustion of single cylinder CI engine. IOP Conf Ser Mater Sci Eng 2016;160:012038. doi:10.1088/1757-899X/160/1/012038.
[27] Lapuerta M, Armas O, García-Contreras R. Effect of ethanol on blending stability and diesel engine emissions. Energy and Fuels 2009;23:4343–54. doi:10.1021/ef900448m.
[28] Kwanchareon P, Luengnaruemitchai A, Jai-In S. Solubility of a diesel-biodiesel-ethanol blend, its fuel properties, and its emission characteristics from diesel engine. Fuel 2007;86:1053–61. doi:10.1016/j.fuel.2006.09.034.
[29] Zöldy M. Ethanol–Biodiesel–Diesel Blends As a Diesel Extender Option on Compression Ignition Engines. Transport 2011;26:303–9. doi:10.3846/16484142.2011.623824.
[30] Hussan MJ, Hassan MH, Kalam MA, Memon LA. Tailoring key fuel properties of dieselebiodieseleethanol blends for diesel engine. J Clean Prod 2013;51:118–25. doi:10.1016/j.jclepro.2013.01.023.
[31] Botero ML, Huang Y, Zhu DL, Molina A, Law CK. Synergistic combustion of droplets of ethanol, diesel and biodiesel mixtures. Fuel 2012;94:342–7. doi:10.1016/j.fuel.2011.10.049.
[32] Avulapati MM, Ganippa LC, Xia J, Megaritis A. Puffing and micro-explosion of diesel-biodiesel-ethanol blends. Fuel 2016;166:59–66. doi:10.1016/j.fuel.2015.10.107.
[33] Avulapati MM, Megaritis T, Xia J, Ganippa L. Experimental understanding on the dynamics of micro-explosion and puffing in ternary emulsion droplets. Fuel 2019;239:1284–92. doi:10.1016/j.fuel.2018.11.112.
[34] Liu Y, Cheng WL, Huo M, Lee CF, Li J, City CC, et al. Effects of Micro-Explosion on Butanol-Biodiesel-Diesel Spray and Combustion. ILASS-Americas 22nd Annu Conf Liq At Spray Syst 2010:2010–2010.
[35] Boggavarapu P, Ravikrishna R V. Evaporating spray characteristics of a diesel-ethanol micro-emulsion. Fuel 2019;246:104–7. doi:10.1016/j.fuel.2019.02.035.
[36] Liu Y, Li J, Jin C. Fuel spray and combustion characteristics of butanol blends in a constant volume combustion chamber. Energy Convers Manag 2015;105:1059–69. doi:10.1016/j.enconman.2015.08.047.
[37] Venu H, Dinesh Babu M. Improvement of ternary fuel combustion with various injection pressure strategies in a toroidal re-entrant combustion chamber. Environ Sci Pollut Res 2018. doi:10.1007/s11356-018-3174-9.
[38] Hagos FY. Fuelling a small capacity agricultural unmodified diesel engine with macro emulsified ethanol , diesel and jatropha derived biodiesel:

performance & emission studies n.d.
[39] Lee KH, Mukhtar MNA, Hagos FY, Noor MM. A study of the stabilities, microstructures and fuel characteristics of tri-fuel (diesel-biodiesel-ethanol) using various fuel preparation methods. IOP Conf Ser Mater Sci Eng 2017;257. doi:10.1088/1757-899X/257/1/012077.
[40] Rajesh S, Kulkarni BM, Banapurmath NR, Kumarappa S. An Experimental Study on performance and emission characteristics of multi cylinder CRDI diesel engine fueled with Ethanol, Acid oil based Biodiesel and Diesel blends. Int J Curr Eng Technol 2017;7:256–65. doi:10.14741/Ijcet/22774106/7.1.2017.40.
[41] Venu H, Madhavan V. Influence of diethyl ether (DEE) addition in ethanol-biodiesel-diesel (EBD) and methanol-biodiesel-diesel (MBD) blends in a diesel engine. Fuel 2017;189:377–90. doi:10.1016/j.fuel.2016.10.101.
[42] Sharanappa P, Navindgi MC. Physico-chemical properties of diesel-biodiesel-ethanol blends 2017;8:506–10.
[43] Cheenkachorn K, Fungtammasan B. An Investigation of Diesel-Ethanol-Biodiesel Blends for Diesel Engine: Part 1. Emulsion Stability and Fuel Properties. Energy Sources, Part A Recover Util Environ Eff 2010;32:637–44. doi:10.1080/15567030903059608.
[44] Khoobbakht G, Najafi G, Karimi M, Akram A. Optimization of operating factors and blended levels of diesel, biodiesel and ethanol fuels to minimize exhaust emissions of diesel engine using response surface methodology. Appl Therm Eng 2016;99:1006–17. doi:10.1016/j.applthermaleng.2015.12.143.
[45] Aydın F, Öğüt H. Effects of using ethanol-biodiesel-diesel fuel in single cylinder diesel engine to engine performance and emissions. Renew Energy 2017;103:688–94. doi:10.1016/j.renene.2016.10.083.
[46] Imdadul HK, Masjuki HH, Kalam MA, Zulkifli NWM, Alabdulkarem A, Rashed MM, et al. Influences of ignition improver additive on ternary (diesel-biodiesel-higher alcohol) blends thermal stability and diesel engine performance. Energy Convers Manag 2016;123:252–64. doi:10.1016/j.enconman.2016.06.040.
[47] Imdadul HK, Masjuki HH, Kalam MA, Zulkifli NWM, Alabdulkarem A, Rashed MM, et al. Higher alcohol-biodiesel-diesel blends: An approach for improving the performance, emission, and combustion of a light-duty diesel engine. Energy Convers Manag 2016;111:174–85. doi:10.1016/j.enconman.2015.12.066.
[48] Júnior LCSS, Ferreira VP, da Silva JAM, Torres EA, Pepe IM. Oxidized biodiesel as a cetane improver for diesel–biodiesel–ethanol mixtures in a vehicle engine. J Brazilian Soc Mech Sci Eng 2018;40. doi:10.1007/s40430-018-1029-4.
[49] Gautam R, Kumar N. Effect of ethanol addition on the properties of Jatropha ethyl ester. Energy Sources, Part A Recover Util Environ Eff 2016;38:3464–9. doi:10.1080/15567036.2016.1145766.
[50] Bahrudin MNHM, Mukhtar AN, Hagos FY, Mamat R, Abdullah AA, Karim ZAA. Comparison between tri-fuel (diesel-ethanol-biodiesel) emulsion with and without surfactant. AIP Conf Proc 2019;2059. doi:10.1063/1.5085999.
[51] Low MH, Mukhtar MNA, Hagos FY, Noor MM. Tri-fuel (diesel-biodiesel-

ethanol) emulsion characterization, stability and the corrosion effect. IOP Conf. Ser. Mater. Sci. Eng., vol. 257, 2017. doi:10.1088/1757-899X/257/1/012082.
[52] Mat Yasin MH, Yusaf T, Mamat R, Fitri Yusop A. Characterization of a diesel engine operating with a small proportion of methanol as a fuel additive in biodiesel blend. Appl Energy 2014;114:865–73. doi:10.1016/j.apenergy.2013.06.012.
[53] Fenouillot F, Cassagnau P, Majesté JC. Uneven distribution of nanoparticles in immiscible fluids: Morphology development in polymer blends. Polymer (Guildf) 2009;50:1333–50. doi:10.1016/j.polymer.2008.12.029.
[54] Fernando S, Hanna M. Development of a novel biofuel blend using ethanol-biodiesel-diesel microemulsions: EB-diesel. Energy and Fuels 2004;18:1695–703. doi:10.1021/ef049865e.
[55] Tolosa LI, Forgiarini A, Moreno P, Salager JL. Combined effects of formulation and stirring on emulsion drop size in the vicinity of three-phase behavior of surfactant-oil water systems. Ind Eng Chem Res 2006;45:3810–4. doi:10.1021/ie060102j.
[56] . LM. Stabilization and Characterization of Heavy Crude Oilin- Water (O/W) Emulsions. Int J Res Eng Technol 2015;03:489–96. doi:10.15623/ijret.2014.0302085.
[57] Wang W, Cheng W, Duan J, Wang P, Gong J. Discussion on the influence of stirring speed on drop size prediction in an oil-water stirring tank using population balance models. Asia-Pacific J Chem Eng 2014;9:309–15. doi:10.1002/apj.1766.
[58] Anisa I., Nour H. Effect of Viscosity and Droplet Diamter on Water-in-Oil Emulsions: An Experimental Study. Eng Technol 2010;38:213–6.
[59] Juttulapa M, Piriyaprasarth S, Takeuchi H, Sriamornsak P. Effect of high-pressure homogenization on stability of emulsions containing zein and pectin. Asian J Pharm Sci 2017;12:21–7. doi:10.1016/j.ajps.2016.09.004.
[60] Li L, Dong W, Xu J, Peng J, Liu Y, Jin D, et al. Effect of high-pressure homogenization preparation on mean globule size and large-diameter tail of oil-in-water injectable emulsions. J Food Drug Anal 2015;23:828–35. doi:10.1016/j.jfda.2015.04.004.
[61] Farzad R, Puttinger S, Pirker S, Schneiderbauer S. Investigation of droplet size distribution for liquid-liquid emulsions in Taylor-Couette flows. J Dispers Sci Technol 2018;39:250–8. doi:10.1080/01932691.2017.1312431.
[62] Hossain ABMS, Boyce AN, Salleh A, Chandran S. Impacts of alcohol type, ratio and stirring time on the biodiesel production from waste canola oil. African J Agric Res 2010;5:1851–9. doi:10.5897/AJAR09.135.
[63] Marinho R, Horiuchi L, Pires CA. Effect of stirring speed on conversion and time to particle stabilization of poly (vinyl chloride) produced by suspension polymerization process at the beginning of reaction. Brazilian J Chem Eng 2018;35:631–9. doi:10.1590/0104-6632.20180352s20160453.
[64] Mashkour MA, Mohammed AA. Impact of mixing speed & reaction time on the biodiesel production from sunflower oil. J Assoc Arab Univ Basic Appl Sci 2016.
[65] Al Basir F, Roy PK. Effects of Temperature and Stirring on Mass Transfer

to Maximize Biodiesel Production from Jatropha curcas Oil: A Mathematical Study . Int J Eng Math 2015;2015:1–9. doi:10.1155/2015/278275.
[66] Afshar Ghotli R, Abdul Aziz AR, Ibrahim S. Effect of Various Curved-Blade Impeller Geometries on Drop Size in a Liquid–Liquid Stirred Vessel. Chem Eng Commun 2017;204:884–96. doi:10.1080/00986445.2017.1325738.
[67] Abidin MIIZ, Raman AAA, Nor MIM. Review on measurement techniques for drop size distribution in a stirred vessel. Ind Eng Chem Res 2013;52:16085–94. doi:10.1021/ie401548z.
[68] Syafiq, Z.Syafiq, Z., Fahmi, O., Awad, O. I., & Adam, A. (2016). The study of stability, combustion characteristics and performance of water in diesel emulsion fuel. MATEC Web of Conferences, 90(X) 1–8. https://doi.org/10.1051/matecconf/20179001022, Fahmi O, Awad OI, Adam A. The study of stability, combustion characteristics and performance of water in diesel emulsion fuel. MATEC Web Conf 2016;90:1–8. doi:10.1051/matecconf/20179001022.
[69] Mahmudul HM, Hagos FY, Mamat R, Noor MM, Yusri IM. Effect of oxygenate additive on diesel engine fuel consumption and emissions operating with biodiesel-diesel blend at idling conditions. IOP Conf Ser Mater Sci Eng 2017;257:012084. doi:10.1088/1757-899X/257/1/012084.
[70] Mahmudul HM, Hagos FY, Mukhtar MNA, Mamat R, Adam Abdullah A. Effect of Alcohol on Diesel Engine Combustion Operating with Biodiesel-Diesel Blend at Idling Conditions. IOP Conf Ser Mater Sci Eng 2018;318. doi:10.1088/1757-899X/318/1/012071.
[71] Jamrozik A, Tutak W, Pyrc M, Sobiepański M. Effect of diesel-biodiesel-ethanol blend on combustion, performance, and emissions characteristics on a direct injection diesel engine. Therm Sci 2017;21:591–604. doi:10.2298/TSCI160913275J.
[72] Yilmaz N, Atmanli A. Experimental assessment of a diesel engine fueled with diesel-biodiesel-1-pentanol blends. Fuel 2017;191:190–7. doi:10.1016/j.fuel.2016.11.065.
[73] S. Fernando, M. Hanna. PHASE BEHAVIOR OF THE ETHANOL-BIODIESEL-DIESEL MICRO-EMULSION SYSTEM. Trans ASAE 2005;48:903–8. doi:10.13031/2013.18494.
[74] Mehta RN, Chakraborty M, Parikh PA. Comparative study of stability and properties of alcohol-diesel blends. Int J Chem Technol 2012;19:134–9.
[75] S. Fernando, M. Hanna. Phase Behavior of the Ethanol-Biodiesel-Diesel Micro-Emulsion System. Trans ASAE 2013;48:903–8. doi:10.13031/2013.18494.
[76] Joshi RM, Pegg MJ. Flow properties of biodiesel fuel blends at low temperatures. Fuel 2007;86:143–51. doi:10.1016/j.fuel.2006.06.005.
[77] Liu H, Hu B, Jin C. Effects of different alcohols additives on solubility of hydrous ethanol/diesel fuel blends. Fuel 2016;184:440–8. doi:10.1016/j.fuel.2016.07.037.
[78] Chen G, Tao D. An experimental study of stability of oil-water emulsion. Fuel Process Technol 2005;86:499–508. doi:10.1016/j.fuproc.2004.03.010.
[79] A. Adam, Abd Rashid Abd Aziz, Ftwi Y. Hagos, M. M. Noor, Kumaran Kadirgama, Rizalman Mamat MMN. The Influence of Formulation Ratio

and Emulsifying Settings on Tri-Fuel (Diesel–Ethanol–Biodiesel) Emulsion Properties. Energies 2019;12:1708. doi:https://doi.org/10.3390/en12091708.
[80] Guo ZG, Wang SR, Wang XY. Emulsification of Bio-Oil Heavy Fraction with Diesel by Mechanical and Ultrasonic Technologies. Appl Mech Mater 2013;316–317:1133–7. doi:10.4028/www.scientific.net/AMM.316-317.1133.
[81] Lin CY, Chen LW. Emulsification characteristics of three- and two-phase emulsions prepared by the ultrasonic emulsification method. Fuel Process Technol 2006;87:309–17. doi:10.1016/j.fuproc.2005.08.014.
[82] Hielscher T. Ultrasonic Production of Nano-Size Dispersions and Emulsions. Ens 2005:14–6. doi:arXiv:0708.1831v1 [cond-mat.mtrl-sci].
[83] Park SH, Kim SH, Lee CS. Mixing stability and spray behavior characteristics of diesel-ethanol- methyl ester blended fuels in a common-rail diesel injection system. Energy and Fuels 2009;23:5228–35. doi:10.1021/ef9004847.
[84] Wu S, Wang G, Ma M, Pang X, Ma J, Jin C, et al. Effects of C3–C5 alcohols on solubility of alcohols/diesel blends. Fuel 2018;236:65–74. doi:10.1016/j.fuel.2018.08.129.
[85] Park SH, Suh HK, Lee CS. Nozzle flow and atomization characteristics of ethanol blended biodiesel fuel. Renew Energy 2010;35:144–50. doi:10.1016/j.renene.2009.06.012.
[86] Badock C, Wirth R, Fath A, Leipertz A. Investigation of cavitation in real size diesel injection nozzles. Int J Heat Fluid Flow 1999;20:538–44. doi:10.1016/S0142-727X(99)00043-0.
[87] Sharma M, Agarwal AK, Bharathi KVL. Characterization of exhaust particulates from diesel engine. Atmos Environ 2005;39:3023–8. doi:10.1016/j.atmosenv.2004.12.047.
[88] Bezergianni S, Dimitriadis A. Comparison between different types of renewable diesel. Renew Sustain Energy Rev 2013;21:110–6. doi:10.1016/j.rser.2012.12.042.
[89] Brosche H. The Arab Oil Embargo and United States Pressure Against Chile : Economic and Political Coercion and the Charter of the United Nations. Case West Reserve J Int Law 1974;7:3–34.
[90] Hamilton JD. Historical Oil Shocks. Natl Bur Econ Res 2011;53:1689–99. doi:10.1017/CBO9781107415324.004.
[91] Brown SPA, Huntington HG. Oil supply disruptions, U.S. economic activity and oil security. Energy Policy 2018;116:297–8. doi:10.1016/j.enpol.2018.02.023.
[92] Demirbas A, Omar Al-Sasi B, Nizami AS. Recent volatility in the price of crude oil. Energy Sources, Part B Econ Plan Policy 2017;12:408–14. doi:10.1080/15567249.2016.1153751.
[93] Nkomo JC. Crude oil price movements and their impact on South Africa. J Energy South Africa 2006;17:25–32.
[94] Ojikutu OT, Onolemhemhen RU, Isehunwa SO. Crude Oil Price Volatility and its Impact on Nigerian Stock Market Performance. Int J Energy Econ Policy 2017;7:302–11.
[95] Fowler L, Neaves TT, Terman JN, Cosby AG. Cultural Penetration and

Punctuated Policy Change: Explaining the Evolution of U.S. Energy Policy. Rev Policy Res 2017;34:559–77. doi:10.1111/ropr.12240.
[96] Gupta E. Oil vulnerability index of oil-importing countries. Energy Policy 2008;36:1195–211. doi:10.1016/j.enpol.2007.11.011.
[97] Yeap GP, Lean HH. Asymmetric inflation hedge properties of housing in Malaysia : New evidence from nonlinear ARDL approach. Habitat Int 2017;62:11–21. doi:10.1016/j.habitatint.2017.02.006.
[98] Prambudia Y, Nakano M. Exploring Malaysia's Transformation to Net Oil Importer and Oil Import Dependence 2012:2989–3018. doi:10.3390/en5082989.
[99] Liew V. Volume 37 , Issue 1 Oil Price Shocks and Sectoral Outputs : Empirical Evidence from Malaysia n.d.;37:38–47.
[100] Saari MY, Dietzenbacher E, Los B. The impacts of petroleum price fluctuations on income distribution across ethnic groups in Malaysia. Ecol Econ 2016;130:25–36. doi:10.1016/j.ecolecon.2016.05.021.
[101] BP. BP Statistical Review of World Energy 2017. Br Pet 2017:8–11. doi:http://www.bp.com/content/dam/bp/en/corporate/pdf/energy-economics/statistical-review-2017/bp-statistical-review-of-world-energy-2017-full-report.pdf.
[102] Atabani AE, Silitonga AS, Badruddin IA, Mahlia TMI, Masjuki HH, Mekhilef S. A comprehensive review on biodiesel as an alternative energy resource and its characteristics. Renew Sustain Energy Rev 2012;16:2070–93. doi:10.1016/j.rser.2012.01.003.
[103] Issariyakul T, Dalai AK. Biodiesel from vegetable oils. Renew Sustain Energy Rev 2014;31:446–71. doi:10.1016/j.rser.2013.11.001.
[104] Rahman MM, Rasul M, Hassan NMS. Study on the tribological characteristics of Australian native first generation and second generation biodiesel fuel. Energies 2017;10. doi:10.3390/en10010055.
[105] Anwar M, Rasul MG, Ashwath N, Rahman MM. Optimisation of Second-Generation Biodiesel Production from Australian Native Stone Fruit Oil Using Response Surface Method. Energies 2018;11. doi:10.3390/en11102566.
[106] Kumar N, Varun, Chauhan SR. Performance and emission characteristics of biodiesel from different origins: A review. Renew Sustain Energy Rev 2013;21:633–58. doi:10.1016/j.rser.2013.01.006.
[107] Shahid EM, Jamal Y. Production of biodiesel: A technical review. Renew Sustain Energy Rev 2011;15:4732–45. doi:10.1016/j.rser.2011.07.079.
[108] Rasul MG, Taweekun J, Ashrafur SM, Mofijur M, Mahlia TMI, Techato K, et al. An Overview of Recent Developments in Biomass Pyrolysis Technologies. Energies 2018;11:3115. doi:10.3390/en11113115.
[109] Bergthorson JM, Thomson MJ. A review of the combustion and emissions properties of advanced transportation biofuels and their impact on existing and future engines. Renew Sustain Energy Rev 2015;42:1393–417. doi:10.1016/j.rser.2014.10.034.
[110] No SY. Application of hydrotreated vegetable oil from triglyceride based biomass to CI engines - A review. Fuel 2014;115:88–96. doi:10.1016/j.fuel.2013.07.001.
[111] Naylor R, Higgins M. The Political Economy of Biodiesel in an Era of Low

Oil Prices. Renew Sustain Energy Rev 2017;77:695–705. doi:10.1016/j.rser.2017.04.026.
[112] Wilman EA. Market Redirection Leakage in the Palm Oil Market. Ecol Econ 2019;159:226–34. doi:10.1016/j.ecolecon.2019.01.014.
[113] Rulli MC, Casirati S, Dell'Angelo J, Davis KF, Passera C, D'Odorico P. Interdependencies and telecoupling of oil palm expansion at the expense of Indonesian rainforest. Renew Sustain Energy Rev 2019;105:499–512. doi:10.1016/j.rser.2018.12.050.
[114] Mahmudul HM, Hagos FY, Mamat R, Adam AA, Ishak WFW, Alenezi R. Production, characterization and performance of biodiesel as an alternative fuel in diesel engines – A review. Renew Sustain Energy Rev 2017;72:497–509. doi:10.1016/j.rser.2017.01.001.
[115] Song H, Quinton K, Peng Z, Zhao H, Ladommatos N. Effects of Oxygen Content of Fuels on Combustion and Emissions of Diesel Engines. Energies 2016;9:28. doi:10.3390/en9010028.
[116] Shahir VK, Jawahar CP, Suresh PR. Comparative study of diesel and biodiesel on CI engine with emphasis to emissions — A review. Renew Sustain Energy Rev 2015;45:686–97. doi:10.1016/j.rser.2015.02.042.
[117] Hoekman SK, Robbins C. Review of the effects of biodiesel on NOx emissions. Fuel Process Technol 2012;96:237–49. doi:10.1016/j.fuproc.2011.12.036.
[118] Shahid E, Jamal Y. Performance evaluation of a diesel engine using biodiesel. Pak J Engg Appl Sci Vol 2011;9:68–75.
[119] Singh G, Singh AP, Agarwal AK. Experimental investigations of combustion, performance and emission characterization of biodiesel fuelled HCCI engine using external mixture formation technique. Sustain Energy Technol Assessments 2014;6:116–28. doi:10.1016/j.seta.2014.01.002.
[120] Salvador FJ, De la Morena J, Martínez-López J, Jaramillo D. Assessment of compressibility effects on internal nozzle flow in diesel injectors at very high injection pressures. Energy Convers Manag 2017;132:221–30. doi:10.1016/j.enconman.2016.11.032.
[121] Ghurri A, Kim JD, Kim HG, Jung JY, Song KK. The effect of injection pressure and fuel viscosity on the spray characteristics of biodiesel blends injected into an atmospheric chamber. J Mech Sci Technol 2012;26:2941–7. doi:10.1007/s12206-012-0703-1.
[122] Sorate KA, Bhale P V. Biodiesel properties and automotive system compatibility issues. Renew Sustain Energy Rev 2015;41:777–98. doi:10.1016/j.rser.2014.08.079.
[123] Gan Y, Lim YS, Qiao L. Combustion of nanofluid fuels with the addition of boron and iron particles at dilute and dense concentrations. Combust Flame 2012;159:1732–40. doi:10.1016/j.combustflame.2011.12.008.
[124] Morganti K, Almansour M, Khan A, Kalghatgi G, Przesmitzki S. Leveraging the benefits of ethanol in advanced engine-fuel systems. Energy Convers Manag 2018;157:480–97. doi:10.1016/j.enconman.2017.11.086.
[125] Lei J, Bi Y, Shen L. Performance and Emission Characteristics of Diesel Engine Fueled with Ethanol-Diesel Blends in Different Altitude Regions. J Biomed Biotechnol 2011;2011:1–10. doi:10.1155/2011/417421.

[126] Park SH, Youn IM, Lim Y, Lee CS. Effect of Bioethanol Blended Diesel Fuel and Engine Load on Spray, Combustion, and Emissions Characteristics in a Compression Ignition Engine. Energy & Fuels 2012;26:5135–45. doi:10.1021/ef300894h.
[127] Srinivasnaik M, Sudhakar TV V, Balunaik B, SomiReddy A. Alcohols as Alternative Fuels for Diesel Engines: A Review. Int J Appl Sci Technol 2015;3:1–8.
[128] Lee S, Lim O. An Investigation on the Spray Characteristics of DME with Variation of Ambient Pressure using the Common Rail Fuel Injection System 2012. doi:10.1007/s12206-012-0806-8.
[129] Ong YOH, Isually KONG V, Esidents IMR. Puffing and micro-explosion behavior in combustion of butanol/ jet A-1 and acetone-butanol-ethanol (A-B-E)/ jet A-1 fuel droplet 2017.
[130] Dürre P. Biobutanol: An attractive biofuel. Biotechnol J 2007;2:1525–34. doi:10.1002/biot.200700168.
[131] Trindade WR da S, Santos RG dos. Review on the characteristics of butanol, its production and use as fuel in internal combustion engines. Renew Sustain Energy Rev 2017;69:642–51. doi:10.1016/j.rser.2016.11.213.
[132] Kasmuri NH, Kamarudin SK, Abdullah SRS, Hasan HA, Som AM. Process system engineering aspect of bio-alcohol fuel production from biomass via pyrolysis: An overview. Renew Sustain Energy Rev 2017;79:914–23. doi:10.1016/j.rser.2017.05.182.
[133] Jin C, Zhang X, Geng Z, Pang X, Wang X, Ji J, et al. Effects of various co-solvents on the solubility between blends of soybean oil with either methanol or ethanol. Fuel 2019;244:461–71. doi:10.1016/j.fuel.2019.01.187.
[134] Aditiya HB, Mahlia TMI, Chong WT, Nur H, Sebayang AH. Second generation bioethanol production: A critical review. Renew Sustain Energy Rev 2016;66:631–53. doi:10.1016/j.rser.2016.07.015.
[135] Zverlov V V., Berezina O, Velikodvorskaya GA, Schwarz WH. Bacterial acetone and butanol production by industrial fermentation in the Soviet Union: Use of hydrolyzed agricultural waste for biorefinery. Appl Microbiol Biotechnol 2006;71:587–97. doi:10.1007/s00253-006-0445-z.
[136] Pereira GCQ, Braz DS, Hamaguchi M, Ezeji TC, Maciel Filho R, Mariano AP. Process design and economics of a flexible ethanol-butanol plant annexed to a eucalyptus kraft pulp mill. Bioresour Technol 2018;250:345–54. doi:10.1016/j.biortech.2017.11.022.
[137] Lapuerta M, García-Contreras R, Campos-Fernández J, Dorado MP. Stability, lubricity, viscosity, and cold-flow properties of alcohol-diesel blends. Energy and Fuels 2010;24:4497–502. doi:10.1021/ef100498u.
[138] Kumar DC, Syam S, Karmakar S, Joarder R. Experimental investigations on nucleation , bubble growth , and micro - explosion characteristics during the combustion of ethanol / Jet A - 1 fuel droplets n.d.
[139] Liu H, Lee CF, Huo M, Yao M. Comparison of ethanol and butanol as additives in soybean biodiesel using a constant volume combustion chamber. Energy and Fuels 2011;25:1837–46. doi:10.1021/ef200111g.
[140] Yilmaz N. Comparative analysis of biodiesel-ethanol-diesel and biodiesel-

methanol-diesel blends in a diesel engine. Energy 2012;40:210–3. doi:10.1016/j.energy.2012.01.079.
[141] Wu H, Nithyanandan K, Zhang J, Lin Y, Lee TH, Lee C fon F, et al. Impacts of Acetone-Butanol-Ethanol (ABE) ratio on spray and combustion characteristics of ABE-diesel blends. Appl Energy 2015;149:367–78. doi:10.1016/j.apenergy.2014.11.053.
[142] Campos-Fernández J, Arnal JM, Gómez J, Dorado MP. A comparison of performance of higher alcohols/diesel fuel blends in a diesel engine. Appl Energy 2012;95:267–75. doi:10.1016/j.apenergy.2012.02.051.
[143] Tongroon M, Suebwong A, Aunchaisri J, Kananont M, Chollacoop N. Combustion Characteristics of Diesohol Fuel in a Modern Diesel Engine. 2018 Third Int. Conf. Eng. Sci. Innov. Technol., IEEE; 2018, p. 1–5. doi:10.1109/ESIT.2018.8665316.
[144] Baltacioglu MK, Kenanoglu R, Aydın K. HHO enrichment of bio-diesohol fuel blends in a single cylinder diesel engine. Int J Hydrogen Energy 2019;126:21. doi:10.1016/j.ijhydene.2019.02.060.
[145] Taib NM, Mansor MRA, Mahmood WMFW, Shah FA, Abdullah NRN. Investigation of diesel-ethanol blended fuel properties with palm methyl ester as co-solvent and blends enhancer. MATEC Web Conf 2016;90. doi:10.1051/matecconf/20179001080.
[146] Thangavelu SK, Ahmed AS, Ani FN. Impact of metals on corrosive behavior of biodiesel-diesel-ethanol (BDE) alternative fuel. Renew Energy 2016;94:1–9. doi:10.1016/j.renene.2016.03.015.
[147] Khoobbakht G, Akram A, Karimi M, Najafi G. Exergy and Energy Analysis of Combustion of Blended Levels of Biodiesel, Ethanol and Diesel Fuel in a di Diesel Engine. Appl Therm Eng 2016;99:720–9. doi:10.1016/j.applthermaleng.2016.01.022.
[148] Shi X, Yu Y, He H, Shuai S, Wang J, Li R. Emission characteristics using methyl soyate–ethanol–diesel fuel blends on a diesel engine. Fuel 2005;84:1543–9. doi:10.1016/j.fuel.2005.03.001.
[149] Shi X, Pang X, Mu Y, He H, Shuai S, Wang J, et al. Emission reduction potential of using ethanol–biodiesel–diesel fuel blend on a heavy-duty diesel engine. Atmos Environ 2006;40:2567–74. doi:10.1016/j.atmosenv.2005.12.026.
[150] Sarkar A, Saha UK. Impact of intake charge preheating on a biogas run dual fuel diesel engine using ternary blends of diesel-biodiesel-ethanol (Paper accepted). J Energy Eng 2018;xxxx:xxxx. doi:10.1061/(ASCE)EY.1943-7897.0000548.
[151] Zhan C, Feng Z, Ma W, Zhang M, Tang C, Huang Z. Experimental investigation on effect of ethanol and di-ethyl ether addition on the spray characteristics of diesel/biodiesel blends under high injection pressure. Fuel 2018;218:1–11. doi:10.1016/j.fuel.2017.12.038.
[152] Guarieiro LLN, de Souza AF, Torres EA, de Andrade JB. Emission profile of 18 carbonyl compounds, CO, CO2, and NOx emitted by a diesel engine fuelled with diesel and ternary blends containing diesel, ethanol and biodiesel or vegetable oils. Atmos Environ 2009;43:2754–61. doi:10.1016/j.atmosenv.2009.02.036.
[153] Armas O, Gómez A, Mata C, Ramos ángel. Particles emitted during the

stops of an urban bus fuelled with ethanol-biodiesel-diesel blends. Urban Clim 2012;2:43–54. doi:10.1016/j.uclim.2012.10.007.
[154] Pang X, Shi X, Mu Y, He H, Shuai S, Chen H, et al. Characteristics of carbonyl compounds emission from a diesel-engine using biodiesel-ethanol-diesel as fuel. Atmos Environ 2006;40:7057–65. doi:10.1016/j.atmosenv.2006.06.010.
[155] Venu H. An experimental assessment on the influence of fuel-borne additives on ternary fuel (diesel–biodiesel–ethanol) blends operated in a single cylinder diesel engine. Environ Sci Pollut Res 2019. doi:10.1007/s11356-019-04739-5.
[156] Corral-Gómez L, Rubio-Gómez G, Martínez-Martínez S, Sánchez-Cruz FA. Effect of diesel-biodiesel-ethanol blends on the spray macroscopic parameters in a common-rail diesel injection system. Fuel 2019;241:876–83. doi:10.1016/j.fuel.2018.12.081.
[157] Tse H, Leung CW, Cheung CS. Investigation on the combustion characteristics and particulate emissions from a diesel engine fueled with diesel-biodiesel-ethanol blends. Energy 2015;83:343–50. doi:10.1016/j.energy.2015.02.030.
[158] Armas O, Martínez-Martínez S, Mata C. Effect of an ethanol-biodiesel-diesel blend on a common rail injection system. Fuel Process Technol 2011;92:2145–53. doi:10.1016/j.fuproc.2011.06.010.
[159] Mahmudul HM, Hagos FY, Mamat R, Abdullah AA. Impact of oxygenated additives to diesel-biodiesel blends in the context of performance and emissions characteristics of a CI engine. IOP Conf Ser Mater Sci Eng 2016;160. doi:10.1088/1757-899X/160/1/012060.
[160] Ibrahim A. Performance and combustion characteristics of a diesel engine fuelled by butanol-biodiesel-diesel blends. Appl Therm Eng 2016;103:651–9. doi:10.1016/j.applthermaleng.2016.04.144.
[161] Zhang ZH, Balasubramanian R. Influence of butanol addition to diesel-biodiesel blend on engine performance and particulate emissions of a stationary diesel engine. Appl Energy 2014;119:530–6. doi:10.1016/j.apenergy.2014.01.043.
[162] Datta A, Mandal BK. A numerical study on the performance, combustion and emission parameters of a compression ignition engine fuelled with diesel, palm stearin biodiesel and alcohol blends. Clean Technol Environ Policy 2017;19:157–73. doi:10.1007/s10098-016-1202-3.
[163] Balamurugan T, Nalini R. Experimental investigation on performance, combustion and emission characteristics of four stroke diesel engine using diesel blended with alcohol as fuel. Energy 2014;78:356–63. doi:10.1016/j.energy.2014.10.020.
[164] Tutak W, Lukács K, Szwaja S, Bereczky Á. Alcohol–diesel fuel combustion in the compression ignition engine. Fuel 2015;154:196–206. doi:10.1016/j.fuel.2015.03.071.
[165] Sathiyamoorthi R, Sankaranarayanan G. The effects of using ethanol as additive on the combustion and emissions of a direct injection diesel engine fuelled with neat lemongrass oil-diesel fuel blend. Renew Energy 2017;101:747–56. doi:10.1016/j.renene.2016.09.044.
[166] Deepankumar S, Gobinath R, Balachandran S. Experimental Investigation

of Performance And Emission Characteristics Of Diesel-Bio Diesel (CSOME) - Ethanol-Diethyl Ether Blends In CI Engine 2017;2:1–5.
[167] Paul A, Panua R, Debroy D. An experimental study of combustion, performance, exergy and emission characteristics of a CI engine fueled by Diesel-ethanol-biodiesel blends. Energy 2017;141:839–52. doi:10.1016/j.energy.2017.09.137.
[168] Rajesh S, Kulkarni BM, Banapurmath NR, Kumarappa S. Effect of injection parameters on performance and emission characteristics of a CRDi diesel engine fuelled with acid oil biodiesel–ethanol blended fuels. Biofuels 2017;0:1–15. doi:10.1080/17597269.2016.1271628.
[169] Yilmaz N, Vigil FM, Donaldson AB, Darabseh T. Investigation of CI engine emissions in biodiesel-ethanol-diesel blends as a function of ethanol concentration. Fuel 2014;115:790–3. doi:10.1016/j.fuel.2013.08.012.
[170] Lin J, Gaustad G, Trabold TA. Profit and policy implications of producing biodiesel-ethanol-diesel fuel blends to specification. Appl Energy 2013;104:936–44. doi:10.1016/j.apenergy.2012.11.049.
[171] Putrasaria Y, Nura A, Muharama A. Performance and emission characteristic on a two cylinder di diesel engine fuelled with ethanol-diesel blends. Energy Procedia 2013;32:21–30. doi:10.1016/j.egypro.2013.05.004.
[172] Aydin H, Ilkiliç C. Effect of ethanol blending with biodiesel on engine performance and exhaust emissions in a CI engine. Appl Therm Eng 2010;30:1199–204. doi:10.1016/j.applthermaleng.2010.01.037.
[173] Randazzo ML, Sodré JR. Exhaust emissions from a diesel powered vehicle fuelled by soybean biodiesel blends (B3-B20) with ethanol as an additive (B20E2-B20E5). Fuel 2011;90:98–103. doi:10.1016/j.fuel.2010.09.010.
[174] Barabás I, Todorut I. Utilization of biodiesel-diesel-ethanol blends in CI engine. Biodiesel-Quality, Emiss By-Products 2011:21. doi:10.5772/27137.
[175] Datta A, Mandal BK. Impact of alcohol addition to diesel on the performance combustion and emissions of a compression ignition engine. Appl Therm Eng 2016;98:670–82. doi:10.1016/j.applthermaleng.2015.12.047.
[176] Kim HJ, Park SH, Lee CS. A study on the macroscopic spray behavior and atomization characteristics of biodiesel and dimethyl ether sprays under increased ambient pressure. Fuel Process Technol 2010;91:354–63. doi:10.1016/j.fuproc.2009.11.007.
[177] Sendzikiene E, Makareviciene V, Janulis P. Influence of fuel oxygen content on diesel engine exhaust emissions. Renew Energy 2006;31:2505–12. doi:10.1016/j.renene.2005.11.010.
[178] LI J. Optimal Mixture Ratios of Biodiesel Ethanol Diesel for Diesel Engines. Energy Power Eng 2011;03:625–9. doi:10.4236/epe.2011.35078.
[179] Zheng Z, Wang XF, Zhong X, Hu B, Liu H, Yao M. Experimental study on the combustion and emissions fueling biodiesel/n-butanol, biodiesel/ethanol and biodiesel/2,5-dimethylfuran on a diesel engine. Energy 2016;115:539–49. doi:10.1016/j.energy.2016.09.054.
[180] Hagos FY, Ali OM, Mamat R, Abdullah AA. Effect of emulsification and blending on the oxygenation and substitution of diesel fuel for compression ignition engine. Renew Sustain Energy Rev 2016.

doi:10.1016/j.rser.2016.11.113.
[181] Tsukahara M, Yoshimoto Y. Influence of Emulsified Fuel Properties on the Reduction of BSFC in a Diesel Engine. SAE Pap 1989;891841. doi:10.4271/891841.
[182] Liang Y, Shu G, Wei H, Zhang W. Effect of oxygen enriched combustion and water-diesel emulsion on the performance and emissions of turbocharged diesel engine. Energy Convers Manag 2013;73:69–77. doi:10.1016/j.enconman.2013.04.023.
[183] Nazha MAA, Rajakaruna H, Crookes RJ. Soot and gaseous species formation in a water-in-liquid fuel emulsion spray—A mathematical approach. Energy Convers Manag 1998;39:1981–9. doi:10.1016/S0196-8904(98)00079-X.
[184] Bidita BS, Suraya AR, Shazed MA, Salleh MAM, Idris A. Preparation, characterization and engine performance of water in diesel nanoemulsions. J Energy Inst 2016;89:354–65. doi:10.1016/j.joei.2015.03.004.
[185] Basha JS, Anand RB. An experimental study in a CI engine using nanoadditive blended water-diesel emulsion fuel. Int J Green Energy 2011;8:332–48. doi:10.1080/15435075.2011.557844.
[186] Sadhik Basha J, Anand RB. Performance, emission and combustion characteristics of a diesel engine using Carbon Nanotubes blended Jatropha Methyl Ester Emulsions. Alexandria Eng J 2014;53:259–73. doi:10.1016/j.aej.2014.04.001.
[187] Fu W, Gong J, Hou L. There is no micro-explosion in the diesel engines fueled with emulsified fuel. Chinese Sci Bull 2006;51:1261–5. doi:10.1007/s11434-006-1261-7.
[188] Shinjo J, Xia J, Ganippa LC, Megaritis A. Physics of puffing and microexplosion of emulsion fuel droplets. Phys Fluids 2014;26. doi:10.1063/1.4897918.
[189] Alvarado, Jorge L HN. Experimental Investigation of Microexplosion Phenomena in emulsified vegetable oil-methanol blends. Proc ASME 2012 Summer Heat Transf Conf 2012:1–8.
[190] Khan MY, Karim ZAA, Aziz a. RA, Tan IM. Experimental investigation of microexplosion occurrence in water in diesel emulsion droplets during the Leidenfrost effect. Energy & Fuels 2014;28:7079–84. doi:10.1021/ef501588z.
[191] Watanabe H, Suzuki Y, Harada T, Matsushita Y, Aoki H, Miura T. An experimental investigation of the breakup characteristics of secondary atomization of emulsified fuel droplet. Energy 2010;35:806–13. doi:10.1016/j.energy.2009.08.021.
[192] Khan MY, Karim ZAA, Aziz ARA, Heikal MR, Crua C. Puffing and Microexplosion Behaviour of Parent - Child Droplets of Water in Pure Diesel Emulsion during Leidenfrost Effect 2016;2202:4–7. doi:http://dx.doi.org/10.1080/00102202.2016.1275593.
[193] Annamalai M, Dhinesh B, Nanthagopal K, SivaramaKrishnan P, Isaac JoshuaRamesh Lalvani J, Parthasarathy M, et al. An assessment on performance, combustion and emission behavior of a diesel engine powered by ceria nanoparticle blended emulsified biofuel. Energy Convers Manag 2016;123:372–80. doi:10.1016/j.enconman.2016.06.062.

[194] Vellaiyan S, Amirthagadeswaran KS. The role of water-in-diesel emulsion and its additives on diesel engine performance and emission levels: A retrospective review. Alexandria Eng J 2016;55:2463–72. doi:10.1016/j.aej.2016.07.021.
[195] Watanabe H, Okazaki K. Visualization of secondary atomization in emulsified-fuel spray flow by shadow imaging. Proc Combust Inst 2013;34:1651–8. doi:10.1016/j.proci.2012.07.005.
[196] Jones S. Bubble nucleation from gas cavities — a review. Adv Colloid Interface Sci 1999;80:27–50. doi:10.1016/S0001-8686(98)00074-8.
[197] Zeng Y, Lee CFF. Modeling droplet breakup processes under micro-explosion conditions. Proc Combust Inst 2007;31 II:2185–93. doi:10.1016/j.proci.2006.07.237.
[198] Zeng Y, Lee C. Modeling of micro-explosion for multicomponent droplets. 11th Int Multidimens Engine Model User's Gr Meet Agenda 2001:1–6.
[199] Ithnin AM, Noge H, Kadir HA, Jazair W. An overview of utilizing water-in-diesel emulsion fuel in diesel engine and its potential research study. J Energy Inst 2014;87:273–88. doi:10.1016/j.joei.2014.04.002.
[200] Li D, Huang Z, Lu XC, Zhang W, Yang J. Physico-chemical properties of ethanol-diesel blend fuel and its effect on performance and emissions of diesel engines. Renew Energy 2005;30:967–76. doi:10.1016/j.renene.2004.07.010.
[201] Shudo T, Nakajima T, Hiraga K. Simultaneous reduction in cloud point, smoke, and NO_x emissions by blending bioethanol into biodiesel fuels and exhaust gas recirculation. Int J Engine Res 2008;10:15–26. doi:10.1243/14680874JER01908.
[202] Geng P, Cao E, Tan Q, Wei L. Effects of alternative fuels on the combustion characteristics and emission products from diesel engines: A review. Renew Sustain Energy Rev 2016. doi:10.1016/j.rser.2016.12.080.
[203] Yuan W, Hansen AC, Zhang Q. Vapor pressure and normal boiling point predictions for pure methyl esters and biodiesel fuels. Fuel 2005;84:943–50. doi:10.1016/j.fuel.2005.01.007.
[204] Kraft D. Particle Formation and Models in Internal Combustion Engines. ComoChengCamAcUk 2014. doi:ISSN 1473-4273.
[205] Kadota T, Tanaka H, Segawa D, Nakaya S, Yamasaki H. Microexplosion of an emulsion droplet during Leidenfrost burning. Proc Combust Inst 2007;31 II:2125–31. doi:10.1016/j.proci.2006.07.001.
[206] Fu G, Zhao C, Liu B, Zhang F, Pang S, Li Y. Investigation on the combustion characteristics of a diesel engine fueled with diesel-azides blends. Appl Energy 2012;91:98–102. doi:10.1016/j.apenergy.2011.09.003.
[207] Sheng HZ, Chen L, Zhang ZP, Wu CK, An C, Cheng CQ. The droplet group microexplosions in water-in-oil emulsion sprays and their effects on diesel engine combustion. Symp Combust 1994;25:175–81. doi:10.1016/S0082-0784(06)80642-9.
[208] Watanabe H, Harada T, Hoshino K, Matsushita Y, Aoki H, Miura T. An experimental investigation of the characteristics of the secondary atomization and spray combustion for emulsified fuel. J Chem Eng Japan 2008;41:1110–8. doi:10.1252/jcej.08we144.
[209] Ocampo-Barrera R, Villasenor R, Diego-Marin A. An experimental study of

the effect of water content on combustion of heavy fuel oil/water emulsion droplets. Combust Flame 2001;126:1845–55. doi:10.1016/S0010-2180(01)00295-4.

[210] Park JW, Huh KY, Park KH. Experimental Study on the Combustion Characteristics of Emulsified Diesel in a RCEM. Seoul 2000 FISITA World Automot Congr 2000:1–6. doi:10.4028/www.scientific.net/AMR.204-210.1351.

[211] Bidita BS, Suraya AR, Shazed MA, Mohd Salleh MA, Idris A. Influence of fuel additive in the formulation and combustion characteristics of water-in-diesel nanoemulsion fuel. Energy and Fuels 2014;28:4149–61. doi:10.1021/ef5002259.

[212] Rakopoulos CD, Giakoumis EG. Simulation and exergy analysis of transient diesel-engine operation. Energy 1997;22:875–85. doi:10.1016/S0360-5442(97)00017-0.

[213] Fahd MEA, Wenming Y, Lee PS, Chou SK, Yap CR. Experimental investigation of the performance and emission characteristics of direct injection diesel engine by water emulsion diesel under varying engine load condition. Appl Energy 2013;102:1042–9. doi:10.1016/j.apenergy.2012.06.041.

[214] Mura E, Massoli P, Josset C, Loubar K, Bellettre J. Study of the micro-explosion temperature of water in oil emulsion droplets during the Leidenfrost effect. Exp Therm Fluid Sci 2012;43:63–70. doi:10.1016/j.expthermflusci.2012.03.027.

[215] Moroianu C, Popescu G. COMBUSTION GRAPHOLOGY USED TO IMPROVE EMULSIONS OF WATER IN HEAVY FUEL OIL. TERMOTEHNICA 1/2008 2008:49–52.

[216] Fu WB, Hou LY, Wang L, Ma FH. A unified model for the micro-explosion of emulsified droplets of oil and water. Fuel Process Technol 2002;79:107–19. doi:10.1016/S0378-3820(02)00106-6.

[217] Ismael MA, Heikal MR, Rashid A, Aziz A, Crua C. An overview of experimental techniques of the investigation of water-diesel emulsion characteristics droplets micro-explosion. ARPN J Eng Appl Sci 2016;11:11975–81.

[218] J. Wilson. Understanding Droplet Size n.d. https://pesticidestewardship.org/pesticide-drift/understanding-droplet-size/.

[219] Mura E, Calabria R, Califano V, Massoli P, Bellettre J. Emulsion droplet micro-explosion: Analysis of two experimental approaches. Exp Therm Fluid Sci 2014;56:69–74. doi:10.1016/j.expthermflusci.2013.11.020.

[220] Zöldy M. The Changes of Burning Efficiency , Emission and Power Output of a Diesel Engine Fueled By Bioethanol – Biodiesel-Diesel Oil Mixtures 2006.

[221] Cheenkachorn K, Fungtammasan B. An Investigation of Diesel-Ethanol-Biodiesel Blends for Diesel Engine: Part 2—Emission and Engine Performance of a Light-Duty Truck. Energy Sources, Part A Recover Util Environ Eff 2010;32:637–44. doi:10.1080/15567030903059608.

[222] Ghadikolaei MA, Cheung CS, Yung K. Study of combustion, performance and emissions of diesel engine fueled with diesel/biodiesel/alcohol blends having the same oxygen concentration. Energy 2018.

doi:10.1016/j.energy.2018.05.164.
[223] Mendes Guedes AD, Leal Braga S, Pradelle F. Performance and combustion characteristics of a compression ignition engine running on diesel-biodiesel-ethanol (DBE) blends – Part 2: Optimization of injection timing. Fuel 2018;225:174–83. doi:10.1016/j.fuel.2018.02.120.
[224] Noorollahi Y, Azadbakht M, Ghobadian B. The effect of different diesterol (diesel–biodiesel–ethanol) blends on small air-cooled diesel engine performance and its exhaust gases. Energy 2018;142:196–200. doi:10.1016/j.energy.2017.10.024.
[225] Shamun S, Belgiorno G, Di Blasio G, Beatrice C, Tunér M, Tunestål P. Performance and emissions of diesel-biodiesel-ethanol blends in a light duty compression ignition engine. Appl Therm Eng 2018;145:444–52. doi:10.1016/j.applthermaleng.2018.09.067.
[226] Pradelle F, Braga SL, Fonseca de Aguiar Martins AR, Turkovics F, Chaar Pradelle RN. Performance and combustion characteristics of a compression ignition engine running on diesel-biodiesel-ethanol (DBE) blends – Potential as diesel fuel substitute on an Euro III engine. Renew Energy 2019;225:174–83. doi:10.1016/j.renene.2019.01.025.
[227] Ghadikolaei MA, Yung K. Effect of Different Fueling Modes on Performance and Emissions of a Diesel Engine Fueled with Diesel-Biodiesel-Ethanol under Different Engine Speeds and Loads Effect of Different Fueling Modes on Performance and Emissions of a Diesel Engine Fueled with Di 2018.
[228] Muralee Krishna S, Abdul Salam P, Tongroon M, Chollacoop N. Performance and emission assessment of optimally blended biodiesel-diesel-ethanol in diesel engine generator. Appl Therm Eng 2019. doi:10.1016/j.applthermaleng.2019.04.012.

APPENDIXES